Available online at www.sciencedirect.com
ScienceDirect
Geochimica et Cosmochimica Acta 74 (2010) 5259–5279
Geochimica et Cosmochimica Acta
www.elsevier.com/locate/gca

The behaviour of Li and Mg isotopes during primary phase dissolution and secondary mineral formation in basalt

Josh Wimpenny [a,*], Sigurður R. Gíslason [b], Rachael H. James [a,1], Abdelmouhcine Gannoun [a,2], Philip A.E. Pogge Von Strandmann [c], Kevin W. Burton [a,3]

[a] Dept. of Earth and Environmental Science, The Open University, Milton Keynes MK7 6AA, UK
[b] Institute of Earth Sciences, University of Iceland, Sturlugata 7, 101 Reykjavik, UK
[c] Bristol Isotope Group, Department of Earth Sciences, University of Bristol, Queens Road, Bristol, BS8 1RJ, UK

Received 4 December 2009; accepted in revised form 21 June 2010; available online 30 June 2010

Abstract

This study presents lithium (Li) and magnesium (Mg) isotope data from experiments designed to assess the effects of dissolution of primary phases and the formation of secondary minerals during the weathering of basalt. Basalt glass and olivine dissolution experiments were performed in mixed through-flow reactors under controlled equilibrium conditions, at low pH (2–4) in order to keep solutions undersaturated (i.e. far-from equilibrium) and inhibit the formation of secondary minerals. Combined dissolution–precipitation experiments were performed at high pH (10 and 11) increasing the saturation state of the solutions (moving the system closer to equilibrium) and thereby promoting the formation of secondary minerals.

At conditions far from equilibrium saturation state modelling and solution stoichiometry suggest that little secondary mineral formation has occurred. This is supported by the similarity of the dissolution rates of basalt glass and olivine obtained here compared to those of previous experiments. The δ^7Li isotope composition of the experimental solution is indistinguishable from that of the initial basalt glass or olivine indicating that little fractionation has occurred. In contrast, the same experimental solutions have light Mg isotope compositions relative to the primary phases, and the solution becomes progressively lighter with time. In the absence of any evidence for secondary mineral formation the most likely explanation for these light Mg isotope compositions is that there has been preferential loss of light Mg during primary phase dissolution.

For the experiments undertaken at close to equilibrium conditions the results of saturation state modelling and changes in solution chemistry suggest that secondary mineral formation has occurred. X-ray diffraction (XRD) measurements of the reacted mineral products from these experiments confirm that the principal secondary phase that has formed is chrysotile. Lithium isotope ratios of the experimental fluid become increasingly heavy with time, consistent with previous experimental work and natural data indicating that ^{6}Li is preferentially incorporated into secondary minerals, leaving the solution enriched in ^{7}Li. The behaviour of Mg isotopes is different from that anticipated or observed in natural systems. Similar to the far from equilibrium experiments initially light Mg is lost during olivine dissolution, but with time the δ^{26}Mg value of the solution becomes increasingly heavy. This suggests either preferential loss of light, and then heavy Mg from olivine, or that the secondary phase preferentially incorporates light Mg from solution. Assuming that the secondary phase is chrysotile, a Mg-silicate, the sense of Mg fractionation is opposite to that previously associated with silicate soils and implies that the fractionation of Mg isotopes during silicate precipitation may be mineral specific. If secondary silicates do preferentially

* Corresponding author. Present address: Geology Department, University of California, One Shields Avenue, Davis, CA 95616, USA. Tel.: +1 510 778 3254.
E-mail address: jbwimpenny@ucdavis.edu (J. Wimpenny).
[1] Present address: National Oceanography Centre, Southampton SO14 3ZH, UK.
[2] Present address: Laboratoire Magmas et Volcans, OPGC, UBP, UMR6524, 5 Rue Kessler 63038 Clermont Ferrand Cedex, France.
[3] Present address: Dept. of Earth Sciences, Oxford University, Oxford OX1 3PR, UK.

0016-7037/$ - see front matter
doi:10.1016/j.gca.2010.06.028

remove light Mg from solution then this could be a possible mechanism for the relatively heavy δ^{26}Mg value of seawater. This study highlights the utility of experimental studies to quantify the effects of natural weathering reactions on the Li and Mg geochemical cycles.

1. INTRODUCTION

The chemical weathering of calcium and magnesium silicates exerts a long term control on the Earth's climate through the consumption of atmospheric CO_2, which in turn drives temperature changes by modifying greenhouse warming (Walker et al., 1981). A number of radiogenic isotope ratios in seawater are sensitive to changes in continental weathering and marine records show that these isotope ratios have varied in the past. For example, the strontium isotope composition ($^{87}Sr/^{86}Sr$) of seawater has become increasingly radiogenic during the Cenozoic (Depaolo and Ingram, 1985; Hess et al., 1986; Richter and Depaolo, 1988) and this has been linked to an increase in the flux of material from continental weathering (Palmer and Elderfield, 1985) resulting in enhanced drawdown of CO_2 and global cooling (Raymo et al., 1988). However, marine radiogenic isotope records, such as Sr, cannot distinguish between changes in the continental weathering flux and changes in source composition that can occur due to changes in the rock type or weathering congruence (Quade et al., 2003). This is crucial because it is principally variations in the silicate weathering rate that influence atmospheric CO_2 consumption on a geological timescale. Consequently, much recent research has turned to other isotope systems that act as tracers of weathering processes, but are much less influenced by variations in lithology.

The stable isotopes of both Li and Mg readily fractionate at the Earth's surface because of the relatively large differences in mass between their isotopes. Unlike Sr the isotope variations of Li and Mg in surface waters are less dependent on differences in lithology. Instead, the major control over both systems is the balance between primary mineral dissolution and secondary mineral formation (Chan et al., 1992; Huh et al., 1998; de Villiers et al., 2005; Kisakurek et al., 2005; Pogge von Strandmann et al., 2006; Tipper et al., 2006b; Wimpenny et al., 2010). During primary mineral dissolution and the formation of secondary minerals it is always the light isotope of Li (^{6}Li) that is taken up into the solid phase, driving the residual fluid to heavy isotope values (Chan et al., 1992; Pistiner and Henderson, 2003; Chan and Hein, 2007). Through this mechanism the dissolved Li isotope composition of river waters (δ^7Li) is always heavier than that of the source bedrock from which the Li is derived. Similarly, the Li composition of seawater [~31‰, (James and Palmer, 2000)] is heavier than its primary sources; continental weathering (~23‰, (Huh et al., 1998)) and high temperature hydrothermal fluids [6–10‰, (Chan et al., 1993, 1994)]. The behaviour of the Mg isotope system is more complex, in that the δ^{26}Mg value of rivers can be strongly influenced by both variations in lithology and secondary mineral formation (Tipper et al., 2006a). Moreover, the formation of secondary silicates can remove both heavy and light Mg from solution (Tipper et al., 2006b; Pogge von Strandmann et al., 2008) while carbonates are always isotopically light relative to the waters from which they precipitate (Galy et al., 2002; Chang et al., 2004). Magnesium in the oceans is derived solely from continental weathering (Berner, 2004) and is removed by a combination of exchange reactions at mid ocean ridges, dolomite formation and the low temperature alteration of clays and detrital sediment (Elderfield and Schultz, 1996; Holland, 2005). The δ^{26}Mg value of seawater (−0.82‰) is slightly higher than estimates of the average riverine input (−1.09‰, (Tipper et al., 2006a)), and it has been suggested that this is either because Mg is not in a steady state in the oceans, or perhaps because light magnesium is preferentially removed during carbonate precipitation (Galy et al., 2002; Holland, 2005; Tipper et al., 2006a). Magnesium is also utilised in biological systems, for example Mg is important to both the chlorophyll molecule and to the function of ATP. Recent work indicates that there is an isotope fractionation associated with the uptake of Mg into chlorophyll and into higher plants (Black et al., 2006; Ra and Kitagawa, 2007; Bi et al., 2008) however, again this Mg fractionation can occur in both senses, similar to its behaviour during mineral reactions. Clearly characterising the behaviour of Mg isotopes in natural systems is challenging because of the range of minerals involved, together with the influence of variables such as temperature, pH, runoff and biology. Because mineral reactions are so important, both in the liberation of elements during the dissolution of primary phases and their uptake during the formation of secondary minerals, it is crucial to understand and quantify how they influence the behaviour of Li and Mg in order to understand how changes in continental weathering might affect the composition of seawater. To this end the behaviour of these isotope systems can be more clearly evaluated in experimental systems where variables such as temperature, pH and saturation state can be controlled.

A number of experimental studies have determined dissolution rates and mechanisms for common rock forming phases such as quartz, feldspar, olivine and basalt glass, over a range of pH, temperature and solution compositions [e.g. (Petrovic, 1976; Petrovich, 1981; Crovisier et al., 1983, 1987; Berger et al., 1988, 1994; Murphy and Helgeson, 1989; Wogelius and Walther, 1992; Oelkers and Schott, 1995; Stillings and Brantley, 1995; Brantley and Stillings, 1996; Stillings et al., 1996; Welch and Ullman, 1996; Daux et al., 1997; Chen and Brantley, 2000; Pokrovsky and Schott, 2000; Rosso and Rimstidt, 2000; Oelkers and Gislason, 2001; Oelkers, 2001a; Gislason and Oelkers, 2003; Liu et al., 2006)]. Similarly, there are many experimental studies that have investigated the precipitation of secondary phases, including such minerals as calcite (Wray and

Daniels, 1957; Zhang and Dawe, 2000), smectite (Harder, 1972), kaolinite (Devidal et al., 1997) and gibbsite (Nagy and Lasaga, 1992). Secondary phase stability in solution is strongly dependent on pH; for example commonly formed secondary phases in rivers such as Fe- and Al-oxyhydroxides are more stable in neutral to high pH solutions (Stefansson and Gislason, 2001), while CO_2 will dissolve more readily in high pH waters (Appelo and Postma, 2005), promoting the formation of secondary carbonates. Temperature is also important, as it directly influences the rates of chemical reactions. Higher temperatures will often lead to enhanced dissolution rates and higher dissolved concentrations which, in turn, leads to higher saturation states of secondary minerals in solution. Thus, due to the sensitivity of both Li and Mg isotopes to secondary mineral formation, both pH and temperature can, indirectly, influence the behaviour of these stable isotope systems. While the rates and mechanisms of mineral reactions and the factors governing secondary mineral formation are relatively well understood, there have been few investigations of isotope behaviour in an experimentally controlled environment.

As yet, the experimental studies that have been undertaken have investigated the isotope changes associated with sorption of Li as well as any isotopic changes associated with bulk rock dissolution (Pistiner and Henderson, 2003; Chan and Hein, 2007; Vigier et al., 2008). There is little measurable fractionation of Li associated with bulk rock dissolution, indicating that fractionation does not occur during primary mineral dissolution (Pistiner and Henderson, 2003). In contrast experimental work supports the results of natural observations that indicate significant fractionation of Li isotopes accompanying incorporation into secondary minerals (Pistiner and Henderson, 2003; Chan and Hein, 2007; Vigier et al., 2008). While there is no fractionation associated with the physical sorption of Li into outer sphere bonds on smectite (Pistiner and Henderson, 2003) the chemical sorption of Li into inner sphere bonds on gibbsite, goethite and smectite is associated with preferential uptake of ^{6}Li (Pistiner and Henderson, 2003; Chan and Hein, 2007; Vigier et al., 2008). All such studies have shown that it is the light isotope (^{6}Li) that is preferentially removed from solution, leaving the resulting fluid enriched in ^{7}Li. Typical fractionation factors during the uptake of Li into clays range between $\alpha = 0.971$–0.999 (Pistiner and Henderson, 2003; Chan and Hein, 2007; Zhang et al., 1998), where α is the fractionation factor calculated from the difference in Li isotopic composition between solid phase and liquid. However, the value of α is dependent on temperature; it is well known that the mass fractionation of stable isotopes will decrease at higher temperatures (Urey, 1947). For example, the fractionation of Li isotopes between clay and solution is 0 to $-11‰$ at high temperature (300–375 °C) but 0 to $-25‰$ at low temperature (4–22 °C) (Vigier et al. (2008) and references within).

The aim of this study is to characterise the behaviour of the Li and Mg isotopes during two of the most important weathering processes that govern surface water chemistry; primary mineral dissolution and secondary mineral formation. To this end, we have conducted a series of experiments involving the dissolution of basalt glass and forsterite under different equilibrium conditions. These minerals have been chosen because they are relatively reactive (Brantley, 2003) and abundant in the Earth's crust (Wolff-Boenisch et al., 2004). Minerals that are most reactive dominate the weathering signal and potentially have the strongest feedback to changes in climate over geological time. The dissolution experiments involve reaction at low pH where secondary phases are unstable (i.e. far from equilibrium). In contrast, the precipitation experiments involve reaction at high pH where the primary phase is undersaturated but secondary phases are supersaturated and more likely to form. To limit the potential number of secondary minerals that could form, particularly clay minerals, only forsterite is used in the precipitation experiments. These experimental results provide some insights into the behaviour of Li and Mg isotopes during weathering reactions, both primary phase dissolution and secondary mineral formation, and provide a basis for understanding and quantifying these isotope systems in the natural environment.

2. METHODS

2.1. Experimental methods

The basalt glass used in these experiments is the same as that used in two previous studies of basalt glass dissolution (Oelkers and Gislason, 2001; Gislason and Oelkers, 2003), where sample preparation is also described in detail. In brief, the chemical composition of the basalt glass is $Na_{0.08}Ca_{0.263}Mg_{0.281}Fe_{0.188}Al_{0.358}SiO_{3.32}$ which is close to the mean composition of oceanic crust and Mid-Ocean Ridge Basalt (MORB) (GERM, 2000). This glass was crushed, ground and sieved to obtain a size fraction of between 40 and 120 μm. Surface area was calculated using the three point Brunauer–Emmett–Teller method (Brunauer et al., 1938), which involves measuring the volume of gas that can be adsorbed onto a mineral surface and so takes surface roughness into account. The basalt glass has a mean BET surface area of 23,000 cm^2/g which is nearly two orders of magnitude greater than the estimated geometric mean of 250 cm^2/g. The forsterite used in these experiments is from San Carlos (gem quality obtained from Wards Natural Sciences); San Carlos olivine has been extensively characterised both in experimental studies [e.g. (Pokrovsky and Schott, 2000; Oelkers, 2001a)] and during isotope analyses of many elements, including Li and Mg [e.g. (Jeffcoate et al., 2007; Teng et al., 2007; Handler et al., 2009)]. San Carlos olivine has an approximate composition of $Mg_{1.82}Fe_{0.18}SiO_4$ (Fo91) (Pokrovsky and Schott, 2000). Crystals were first handpicked and then crushed using an agate mortar, and subsequently milled and sieved to obtain grains of between 40 and 120 μm. Forsterite grains were then ultrasonically cleaned in acetone; this cleaning step was repeated until all fines were removed before drying overnight at 60 °C. The surface area of forsterite powder has been estimated previously (Pokrovsky and Schott, 2000; Oelkers, 2001a) using similar forsterite ground to the same size fraction. The estimated BET surface area is 800 cm^2/g.

All experiments were performed in mixed through-flow reactors, where fluid is constantly pumped through the stirred reactors as illustrated in Fig. 1. The dissolution experiments were carried out in titanium reactors with a volume of 300 ml, where both temperature and pressure can be controlled. The temperature ranged from 25 to 55 °C and was controlled by a Parr heating sleeve, while pressure was maintained at atmospheric levels for all experiments. Fluid was supplied to the reactor via a high precision HPLC pump which provided a continuous flow of between 1 and 8 g/min during the experiments. A motorised stirrer was used to hold the reacting mineral in solution thereby aiding the dissolution process by ensuring that the reacting surfaces remain exposed. Stirring also prevents the dissolution becoming dependent on the rate of diffusive transport away from mineral surfaces. Gislason and Oelkers (2003) showed that at pH 2–3 stir rates should be kept above 550 and 350 rpm, respectively, to ensure that dissolution rates are surface reaction controlled. Consequently all experiments were performed with a stir speed of over 350 rpm. The dissolution experiments were performed at low pH (2–4); low pH inlet solutions were created by mixing suprapure HCl with an ammonium chloride buffer. All solutions were prepared to an ionic strength of 0.01 mol/kg. Fluids were then sampled via a 1 μm titanium filter which prevents the loss of solid particles from the reactor. Prior to sample collection the fluid was also passed through a 0.2 μm sterile acetate filter as shown in Fig. 1.

Dissolution–precipitation experiments were performed in polypropylene reactors, with volumes of 250 ml, which have no internal temperature control. Temperatures of between 25 and 75 °C were maintained by placing the reactors in a temperature controlled water bath (Fig. 1). Fluid was pumped into the reactors via a peristaltic pump with flow rates ranging from 0.15 to 4 g/min. The solution is output from the reactor via a 1 μm steel filter to ensure that solid particles are not lost. Prior to sampling the solution was passed through a sterile acetate 0.2 μm filter. There is no in-built stirring mechanism within the polypropylene reactors so Teflon coated magnetic stirrers were used to stir the solution throughout the experiment. Floating stir bars were used in order to prevent grinding of the solid phase and hence inadvertently increase its surface area during the experiment. As for the dissolution experiments, solutions were prepared to an ionic strength of 0.01 mol/kg. Because high pH values were needed a combination of NH_4Cl and NH_4OH was used in order to obtain pH values of 10 and 11, respectively. At these high pH values the precipitation of carbonates is a possibility because the dominant carbonic acid species is CO_3^{2-}; in order to prevent carbonate precipitation the input solutions were kept in a mantle of nitrogen gas.

All apparatus was acid cleaned and rinsed with deionised water prior to starting each experiment. Between 2 and 10 g of mineral phase was added to the reactor vessel before filling with 0.01 mol/kg solution at the desired pH. In the dissolution experiments, the lowest pH value was attained last because this causes the most alteration of the sample and thus could cause the greatest change in the mineral surface area. Before sampling of the fluids three reactor residence times were left to allow the system to attain a mechanical steady state. One residence time is defined as the time taken for fluid to fill each reactor once and is dependent on the flow rate of the inlet solution. On changing any of the experimental parameters such as pH and temperature another three residence times were left before sampling was resumed. Samples of 100 ml from both dissolution and precipitation experiments were collected in acid cleaned 125 ml PTFE sample tubes and a small proportion of each unacidified sample was tested for pH. Samples were also weighed in order to calculate actual flow rates. All samples were then acidified using suprapure grade HNO_3 to a concentration of 0.5% in readiness for later ICP-AES analysis.

2.2. Analytical methods

2.2.1. Concentration measurements

Major element concentrations for all solutions were measured by ICP-AES at the University of Iceland. Acidified solutions were run alongside an in house standard; a natural water sample from the Selsund region of Iceland,

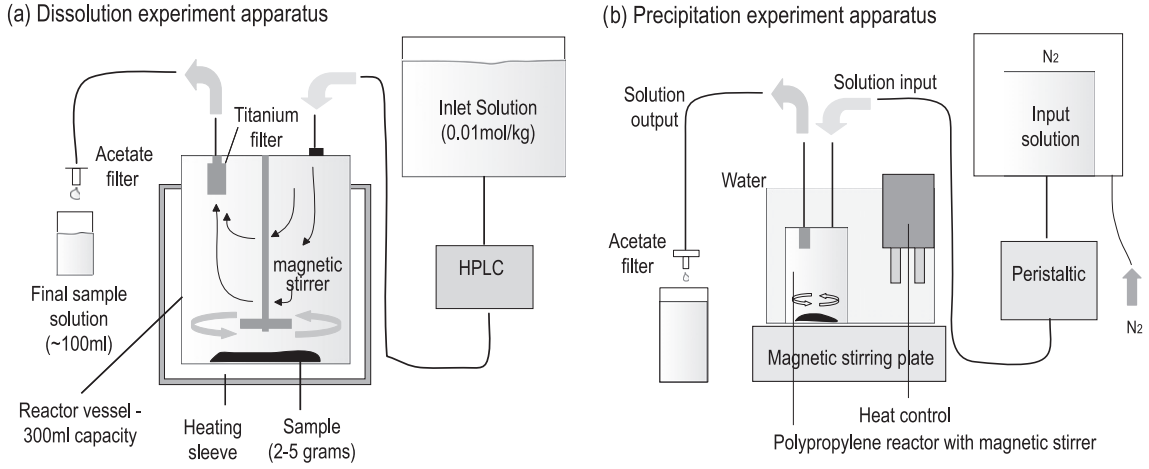

Fig. 1. A schematic diagram showing the experimental apparatus used for (a) dissolution experiments and (b) precipitation experiments.

calibrated against SPEX Certiprep single element standards. Duplicate measurements of the experimental solutions yielded relative errors of less than 5%. All minor and trace element concentrations were measured by ICP-MS at the Open University. Multi element standards were made up using single element standard solutions with a concentration of 1000 ppm; these were diluted to the required standard concentration using 2% TD (Teflon distilled) HNO_3. Analyses of standard solutions with variable but known concentrations enabled the construction of a calibration curve. These standard solutions included the following minor and trace elements: Li, Fe, Cr, Zn, Cu, Rb, Sr, Ba as well as the rare earth elements (REE). The in house standard Sco2/15 (Scottish river water) and the riverine standard SLRS-4 (Ottawa river water, NRCC) were used to monitor and correct for any machine drift. External reproducibility as determined from repeat measurements of SLRS-4 is better than 8% (2σ).

Mineral phases were dissolved using a mixture of TD HNO_3 and Aristar HF. Dissolved samples were dried and redissolved in a mixture of TD HNO_3 and MQ water to an acid strength of 2%. Concentrations were then measured by ICP-MS. All measurements were calibrated using a series of rock standard reference materials; in this case JB-2 (JGS basalt), BIR-1 (USGS basalt), BHVO-1 (USGS basalt), BCR-2 (USGS basalt), AGV-1 (USGS andesite), W-2 (USGS diabase), G-2 (USGS granite), SDC-1 (USGS mica-schist) and JG-2 (JGS granite). Two standards (JB-2 and BIR-1) were routinely measured to assess external reproducibility; the 2σ external error is <6% for all major (JB-2) and minor (BIR-1) element analyses.

2.2.2. Isotope chemistry

For Li isotope analysis a minimum of 5 ng of Li was separated from the sample matrix by cation exchange chromatography, following the technique of James and Palmer (2000). The cation columns used in this study are Teflon with an internal diameter of 6 mm and they are loaded with 2.4 ml of Bio-Rad AG50W-X12 (200–400 mesh) cation exchange resin to a resin height of 8.5 cm. The sample is then eluted using 0.2 N TD HCl, collected, dried down and then redissolved in 3% TD HNO_3 for analysis by multi collector inductively coupled plasma mass spectrometry (MC-ICP-MS). Total procedural Li blanks were ~12 pg. The Li isotope procedure for low concentration samples performed at Bristol uses a similar method, but with a second column (0.25 ml resin volume) to remove residual matrix and matrix introduced by the larger volume of resin in the first column.

Magnesium was also separated from the sample matrix by cation exchange chromatography using the same column setup as for Li. A minimum of 500 ng of Mg was loaded onto the columns and eluted with a combination of 0.75 N and 2 N TD HCl. The major difference between the Li and Mg techniques is that for Mg all rock samples were first processed through an anion column to remove any potential interference from iron following the technique of Wiechert and Halliday (2007). The anion columns used were Teflon with an internal diameter of 6 mm. The anion resin used was Bio-Rad AG1-X8 (200–400 mesh). Rock samples were dried down, taken up in 6 N HCl and passed through the anion columns to remove Fe before being processed through cation columns. Finally, all samples are dried down and redissolved in 3% TD HNO_3 for analysis by MC-ICP-MS. Total procedural Mg blanks were ~50 pg.

2.2.3. Isotope analyses

All Mg isotope measurements were made on a Thermo Finnigan Neptune while Li isotope measurements were performed on a Nu-Instruments MC-ICP-MS at the Open University. A number of low-level Li samples were also processed and analysed on a Thermo Finnigan Neptune at the University of Bristol.

2.2.3.1. Lithium. Lithium samples were analysed with a Li concentration of 10 ppb. On the Nu-Plasma (run in conjunction with a Nu-DSN desolvating nebuliser) this yielded a signal with ^7Li intensity of 1 V and a background of ~6 mV of ^7Li or 0.6% of the total sample beam. Each sample run consisted of 1 block of 20 measurements, and used 0.5 ml of sample solution. Consequently, samples consisting of 5 ng of Li could be run at 10 ppb for a single analysis. However, where possible at least 10 ng of Li was processed, enabling one repeat isotope measurement to be made. Each sample run was preceded by measuring the on-peak blank of the 3% HNO_3 solution. The blank was subtracted from the sample measurement online. Isotope ratios are expressed as δ^7Li, which is the permil (‰) difference from the standard LSVEC. Results are calculated using the standard-sample bracketing technique where $\delta^7Li = \{[(^7Li/^6Li)_{sample}/(^7Li/^6Li)_{standard}]-1\} \times 1000$. Typically, the internal precision attained with the Nu-Plasma was better than 0.2‰ (2σ). External reproducibility was assessed from repeat preparations ($n = 8$) and repeat measurements of seawater ($n = 40$). The average seawater δ^7Li was 31.08 ± 0.82‰ (2σ), which compares favourably with previously published values (Chan and Edmond, 1988; James and Palmer, 2000; Millot et al., 2007). To validate the accuracy of low level Li analyses, several solutions containing <10 ng of Li were also analysed at the University of Bristol using a Thermo Finnegan Neptune MC-ICP-MS. This yields a ^7Li intensity of ~1 V for a 1 ppb Li beam, compared to a background of ~10–20 mV. Analyses were performed as detailed in Jeffcoate et al. (2004) and Marschall et al. (2007). The internal precision of these measurements (2σ) was similar to that achieved at the Open University (~0.2‰), and the long-term external precision (based on repeated; $n = 15$, chemistry = 15) is ±0.4‰ (2sd) for 1–4 ng of Li.

2.2.3.2. Magnesium. Magnesium samples were analysed with a Mg concentration of 500 ppb at medium resolution with a wet plasma. A typical ^{26}Mg signal for a 500 ppb sample was between 10 and 12 V; the blank (3% HNO_3 solution) typically gave <0.01 V of ^{26}Mg; this was subtracted offline during data processing. Isotope measurements are expressed as $\delta^{26}Mg$, which is the ‰ difference from the standard DSM-3. Results are calculated using the standard-sample bracketing technique where $\delta^{26}Mg = \{[(^{26}Mg/^{24}Mg)_{sample}/(^{26}Mg/^{24}Mg)_{standard}]-1\} \times 1000$. Typically the internal precision of $\delta^{26}Mg$ measurements (2σ) was better than 0.05‰,

and the internal precision of δ^{25}Mg measurements (2σ) was better than 0.03‰. In order to monitor the external reproducibility of the magnesium isotope measurements the standard CAM-1 was routinely measured at least 2–3 times during an analytical session. The average δ^{26}Mg composition of CAM-1 measured over the course of this study ($n = 22$) is -2.60 ± 0.11‰ (2σ) while the average δ^{25}Mg composition is -1.35 ± 0.06‰ (2σ), which compares favourably with values for CAM-1 measured elsewhere [−2.58‰ (Young and Galy, 2004; Pearson et al., 2006)].

3. RESULTS

3.1. Mineral phases

The elemental concentrations of both unreacted and reacted mineral phases are presented in Tables 1 and 2. By comparing the concentration of elements in the reacted phase with the concentrations in the unreacted mineral the % loss during dissolution can be calculated. Experiment BG1 (pH2, 25 °C) has the highest % loss of each element; the elements with the greatest % loss were Li, Al, and Mg with losses of 12%, 11.5% and 10.5%, respectively. In general these elements were the most readily lost in all of the basalt glass experiments while Ti and Cr concentrations remained similar to those before reaction. Unreacted basalt glass has a Li concentration of 4.7 ppm and an Mg concentration of 6 wt%. In the forsterite experiments most elements were below the calibration range with Al, K, Na amongst the elements that could not be measured. The element with the greatest loss during the experiments was Li with a loss of ~17% relative to the levels in the unreacted forsterite (Table 2). The initial forsterite Li concentration is lower than that of basalt glass with a concentration of 2 ppm.

3.2. Dissolution experiments

3.2.1. Dissolution rates

All dissolution rates (r) have been calculated from the dissolved Si concentration using the following equation:

$$r = \frac{\mathrm{Si_{out}} \times F}{S_{\mathrm{BET}}} \quad (1)$$

where r, dissolution rate (mol/cm^2/s); Si($_{\mathrm{out}}$), outlet Si concentration (mol/kg); F, fluid flow rate (g/s); S($_{\mathrm{BET}}$), surface area of sample powder determined by BET method.

There was no measurable dissolved silica in the inlet solution. Far from equilibrium dissolution rates of basalt glass and forsterite are presented in electronic annex EA-1 and EA-2, respectively. The dissolution rates of basaltic glass and forsterite are dependent on temperature and pH; dissolution rates increase with temperature and as pH decreases from 4 to 2. Dissolution rates obtained in these experiments closely match those reported previously using similar experimental conditions (Table 3). The dissolution rate of forsterite, normalized to BET surface area, is generally faster than basalt glass at an equivalent pH. For example at pH 3 the dissolution rate of forsterite is $\sim 4.5 \times 10^{-13}$ mol/cm^2/s while the dissolution rate of basalt glass is $\sim 5.5 \times 10^{-14}$ mol/cm^2/s.

The dissolution rate of forsterite in pH 2 solutions also varies depending on the stir speed used. A sharp rise in Si concentration from ~5 to ~10 ppm occurs when the stir speed increases from 350 to 550 rpm. This equates to an increase in the dissolution rate by a factor of 2.

3.2.2. Lithium and magnesium isotopes

Lithium concentrations during the dissolution of basalt glass range from 0.03 ppb in pH 4 solutions to 0.5 ppb in pH 2 solutions. In comparison, during the dissolution of forsterite, Li concentrations range from 0.01 to 0.1 ppb in pH 4 and 2 solutions, respectively. The Li concentration needs to be at least 0.05 ppb in order to obtain a single isotope measurement; consequently it was not possible to measure the Li isotope ratio of the fluid phase for some of the sample solutions.

Magnesium concentrations are significantly higher because this element is a major constituent of both forsterite and basalt glass. During the dissolution of basalt glass Mg concentrations ranged from 30 to 6000 ppb at pH 4

Table 1
Element concentrations for unreacted and reacted mineral/glass phases. Concentrations of Na, Al, and K in forsterite were below the calibration range. Concentrations of Mg were above the calibration range.

Sample	Na (wt%)	Mg (wt%)	Al (wt%)	K (wt%)	Ca (wt%)	Ti (ppm)	Cr (ppm)	Mn (ppm)	Fe (wt%)
Basalt glass	1.53	6.02	8.43	0.22	6.89	9455	530	1500	8.64
Forsterite					0.03	21	212	1020	7.19
BG1	1.41	5.40	7.47	0.21	6.41	10200	541	1380	8.20
BG2	1.45	5.47	7.80	0.22	6.66	9340	569	1450	8.41
BG3	1.55	5.90	8.32	0.24	7.19	9940	564	1550	9.04
BG4	1.53	5.77	8.15	0.23	7.00	9540	524	1500	8.77
BG5	1.50	5.74	7.99	0.22	6.80	10000	510	1470	8.67
FO1					0.04	50	207	1000	7.16
FO2					0.04	38	201	990	7.09
FO3					0.03	20	191	954	6.90
FO4					0.04	27	215	1000	7.28
FO5					0.04	18	242	995	7.17
FO6					0.04	19	268	980	7.05
FO7					0.04	20	219	1000	7.19

The San Carlos olivine used in this study has an approximate composition of $Mg_{1.82}Fe_{0.18}SiO_4$ (Fo9; (Pokrovsky and Schott, 2000) and the Stapafell basaltic glass $Na_{0.08}Ca_{0.263}Mg_{0.281}Fe_{0.188}Al_{0.358}SiO_{3.32}$ (Oelkers and Gislason, 2001).

Table 2
Lithium elemental and isotope data for initial and reacted mineral/glass phases and experimental solutions. *Isotopic analyses performed at the University of Bristol.

Minerals and glass	Experiment type	Time (h)	pH	T (°C)	[Li] (ppm)	δ^7Li (‰)	Internal error (2σ)
Basalt glass	N/A				4.73	5.82	0.31
Forsterite	N/A				2.05	1.57	0.12
BG1	Dissolution		2	25	4.17	6.13	0.11
BG2	Dissolution		3–4	25	4.36	5.93	0.14
BG3	Dissolution		4	25	4.7	4.96	0.16
BG4	Dissolution		4	35–55	4.52	4.76	0.13
BG5	Dissolution		3	25–55	4.54	4.81	0.16
FO1	Dissolution		2–4	25	1.79	2.03	0.16
FO2	Dissolution		3–4	25	1.76	2.08	0.15
FO3	Precipitation		10	25	1.61	2.05	0.17
FO4	Dissolution		3	25–55	1.72	2.10	0.15
FO5	Precipitation		11	25	1.63	2.68	0.13
FO6	Precipitation		10	75	1.72	2.80	0.15
FO7	Precipitation		11	75	1.68	2.32	0.15
Solutions					[Li] (ppb)		
FO2-A	Dissolution	6	3	25	0.09	1.44	0.53
FO2-B*	Dissolution	12	3	25	0.03	1.70	0.26
FO2-H	Dissolution	47	2	25	0.06	0.51	0.21
FO2-J*	Dissolution	55	2	25	0.06	3.20	0.25
FO2-K	Dissolution	66	2	25	0.09	2.70	0.24
FO2-N	Dissolution	78	2	25	0.10	0.70	0.18
FO3-A	Precipitation	15	10	25	0.12	2.03	0.11
FO3-G	Precipitation	51	10	25	0.18	4.41	0.10
FO3-L	Precipitation	122	10	25	0.52	8.46	0.15
FO3-R	Precipitation	232	10	25	2.62	8.21	0.12
FO5-A	Precipitation	11	11	25	0.15	9.41	0.24
FO5-B	Precipitation	16	11	25	0.17	10.61	0.09
FO5-G	Precipitation	87	11	25	2.79	10.13	0.06
FO5-L	Precipitation	207	11	25	2.62	10.69	0.09
FO6-A	Precipitation	16	10	75	2.61	9.49	0.17
FO6-B	Precipitation	22	10	75	2.96	9.25	0.09
FO6-G	Precipitation	64	10	75	2.16	10.74	0.07
FO6-N	Precipitation	118	10	75	1.27	11.04	0.09
FO6-O	Precipitation	173	10	75	1.52	10.79	0.10
FO6-S	Precipitation	218	10	75	1.16	10.66	0.10
FO7-A	Precipitation	10	11	75	3.79	7.26	0.20
FO7-B	Precipitation	18	11	75	3.76	8.68	0.11
FO7-H	Precipitation	64	11	75	2.38	10.82	0.07
FO7-J	Precipitation	130	11	75	1.87	12.2	0.07
FO7-N	Precipitation	178	11	75	1.45	12.19	0.09
BG5-E	Dissolution	15	3	25	0.13	2.99	0.11
BG5-G*	Dissolution	25	3	35	0.10	3.3	0.11
BG5-J	Dissolution	34	3	35	0.11	2.43	0.06
BG5-O	Dissolution	49	3	45	0.07	2.47	0.08
BG5-Q*	Dissolution	53	3	55	0.06	2.4	0.14
BG5-T	Dissolution	62	3	55	0.07	3.46	0.18
BG2-B*	Dissolution	24	4	25	0.04	5.0	0.14
BG2-E*	Dissolution	59	4	25	0.04	3.5	0.43
BG2-F	Dissolution	61	3	25	0.10	2.5	0.19
BG2-H	Dissolution	64	3	25	0.13	3.4	0.23
BG2-J	Dissolution	67	3	25	0.12	2.85	0.16

and 2, respectively. Higher concentrations were obtained during the dissolution of forsterite; ranging from 800 ppb at pH 4 to 19,000 ppb at pH 2.

The Li isotope results are shown in Table 2 and Fig. 2. The Li isotope ratio of unreacted basalt glass is between 5‰ and 6‰, while reacted glass has an almost identical δ^7Li composition of between 4.8‰ and 6‰. In comparison the experimental solutions possess slightly lighter δ^7Li compositions, where solutions from BG5 and BG2 have δ^7Li values that range between 2.4‰ and 3.5‰. The Li isotope ratio of unreacted forsterite is around 1.5‰ while reacted forsterite has δ^7Li values of 2–2.1‰. Only four experimental solutions could be measured because of low Li concentrations. These solutions have δ^7Li values of between 0.5‰ and 2.7‰, similar to the composition of forsterite given the reported uncertainties (Fig. 2).

Table 3
Comparison of dissolution rates (at 25 °C) obtained in this study with previous work.

	$-\log r$				
pH	This study	Pokrovsky et al. (2004)	Oelkers (2001a,b)	Rosso and Rimstidt (2000)	Wogelius and Walther (1992)
Forsterite experiments					
~2.1	11.6	11.7	11.9	11.86	12.15
~3.1	12.2	12.15		12.1	12.8
~4.4	12.9	12.7–12.8		12.6	13.1
10.3	14.5	14.7			
11	14.5	14.6			
Basalt glass experiments					
pH	This study	Gislason and Oelkers (2003)			
2.1	11.92	11.9			
3.4	13.1	13.1			
4.5	14.7	14.17			

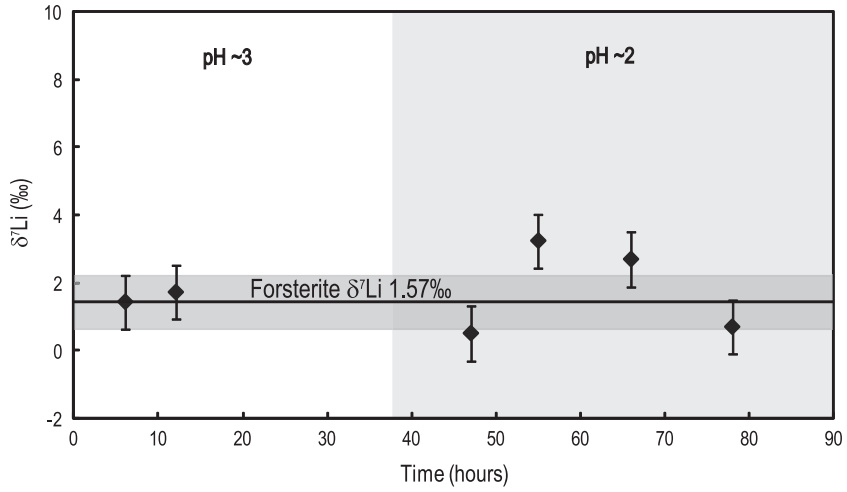

Fig. 2. Lithium isotope ratios of forsterite and experimental fluids during experiment FO2 (pH 2–3, 25 °C). Error bars show the external reproducibility (2σ).

The Mg isotope results are shown in Table 4 and Fig. 3. The Mg isotope ratio of unreacted and reacted basalt glass is around −0.3‰. Unreacted forsterite has a similar Mg isotope composition to basalt glass (δ^{26}Mg −0.26‰) while reacted forsterite has a slightly lower δ^{26}Mg value of −0.32‰. In comparison, the composition of the experimental fluid is always isotopically lighter than the dissolving mineral or glass (Fig. 3). During experiments BG5 (pH 3, 25–55 °C) and FO2 (pH 2–3, 25 °C) both solutions evolve from initial Mg isotope ratios of around −0.47‰ to increasingly light δ^{26}Mg values of around −0.62‰ by the end of the experiment.

3.3. Secondary phase precipitation experiments

3.3.1. Dissolution rates

The dissolution–precipitation experiments involved the dissolution of forsterite at high pH and the precipitation of a secondary mineral. The dissolution rate of forsterite is far lower at pH 10–11 than at pH 2–4, consistent with previous studies (Wogelius and Walther, 1991; Pokrovsky and Schott, 2000). In experiment FO3 at pH 10 the system maintains a relatively constant dissolution rate for the first 130 h, as can be seen in Fig. 4. During this period the flow rate varied from 4 to 1 g/min. When the flow rate falls further, to 0.15 g/min, the dissolution rate also falls to 3.16×10^{-15} mol/cm^2/s (Fig. 4) indicating increased silica consumption by secondary products with time. A similar pattern of change is observed during experiment FO5 (pH 11), at a flow rate of 3 g/min the dissolution rate remained at a constant value of 2.82×10^{-14} for 24 h, and after decreasing the flow rate to 0.2 g/min the dissolution rate also fell to 3.16×10^{-15} mol/cm^2/s.

These high pH experiments were repeated at 75 °C. The dissolution rate is higher than at 25 °C, with the experiment at pH 10 having the higher rate of 3.98×10^{-14} mol/cm^2/s compared to 1.41×10^{-14} mol/cm^2/s at pH 11 (electronic annex EA-3).

3.3.2. Lithium and magnesium isotopes

During the dissolution–precipitation experiments Li isotope ratios in the solution become heavier with time, and are always heavier than the starting olivine. For example after the first 15 h at pH 10 and 25 °C (FO3) the solution

Table 4
Magnesium isotope data for forsterite, glass and experimental solutions.

Minerals and glass	Exp. type	Time (min)	pH	T (°C)	[Mg] wt%	δ^{26}Mg (‰)	Internal Error (2σ)	δ^{25}Mg (‰)	Internal error (2σ)
Basalt glass					6.02	−0.30	0.02	−0.15	0.02
Basalt glass					6.02	−0.31	0.03	−0.16	0.02
Forsterite 1						−0.24	0.03	−0.12	0.02
Forsterite 2						−0.26	0.02	−0.15	0.02
Forsterite 3						−0.26	0.02	−0.13	0.02
BG1	Dissolution		2	25	5.40	−0.35	0.03	−0.18	0.02
BG5	Dissolution		3	25–55	5.74	−0.31	0.03	−0.16	0.02
FO1	Dissolution		2–4	25		−0.34	0.02	−0.19	0.02
FO5	Precipitation		11	25		−0.31	0.02	−0.15	0.02
Solutions					[Mg] (ppm)				
BG5-E	Dissolution	780	3	25	1.44	−0.51	0.04	−0.24	0.02
BG5-J	Dissolution	1950	3	35	1.02	−0.51	0.07	−0.25	0.04
BG5-N	Dissolution	2670	3	45	0.55	−0.58	0.06	−0.29	0.04
BG5-T	Dissolution	3600	3	55	0.46	−0.62	0.06	−0.31	0.03
FO2-D	Dissolution	1440	3	25	2.70	−0.44	0.05	−0.21	0.03
FO2-F	Dissolution	2160	3	25	2.95	−0.45	0.04	−0.24	0.03
FO2-I	Dissolution	3060	2	25	7.00	−0.54	0.05	−0.27	0.03
FO2-M	Dissolution	4440	2	25	16.5	−0.62	0.03	−0.31	0.02
FO3-A	Precipitation	900	10	25	0.01	−0.54	0.09	−0.27	0.05
FO3-G	Precipitation	3060	10	25	0.09	−0.50	0.04	−0.25	0.03
FO3-L	Precipitation	7320	10	25	0.24	−0.39	0.05	−0.20	0.03
FO3-R	Precipitation	13925	10	25	0.29	−0.34	0.03	−0.17	0.02
FO5-B	Precipitation	937	11	25	0.07	−0.65	0.04	−0.33	0.03
FO5-E	Precipitation	2239	11	25	0.15	−0.43	0.04	−0.21	0.03
FO5-H	Precipitation	6578	11	25	0.11	−0.27	0.03	−0.15	0.02
FO5-L	Precipitation	12364	11	25	0.09	−0.23	0.03	−0.14	0.02
FO6-A	Precipitation	930	11	75	0.26	−0.30	0.02	−0.17	0.02
FO6-F	Precipitation	3150	11	75	0.22	−0.22	0.02	−0.13	0.02
FO6-N	Precipitation	7085	11	75	0.19	−0.21	0.02	−0.12	0.02
FO6-R	Precipitation	12475	11	75	0.35	−0.21	0.02	−0.12	0.02

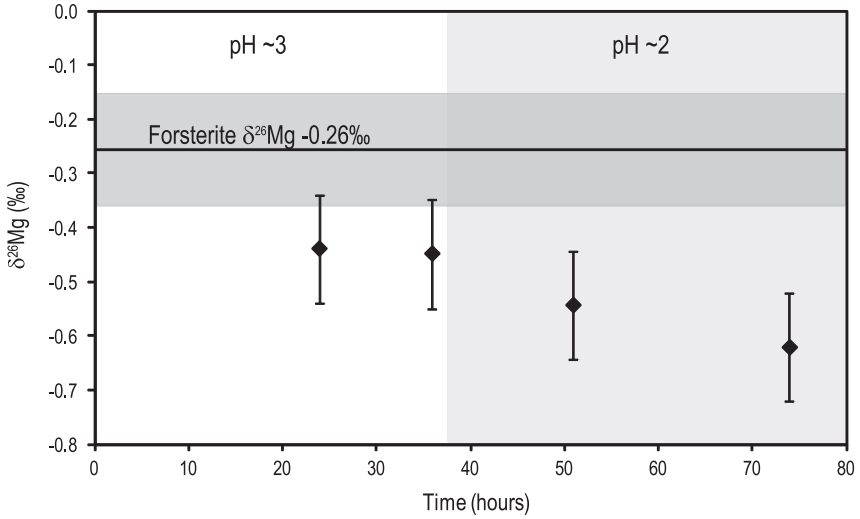

Fig. 3. Magnesium isotope ratio of experimental fluids during experiment FO2 (pH 2–3, 25 °C). Error bars show the external reproducibility (2σ).

had a δ^7Li value of 2‰, and over the next 200 h the Li isotope ratio increased to 8.4‰ (Fig. 5). In experiment FO5 (pH 11 and 25 °C) the δ^7Li value of the solution was 9.4‰ after 10 h of the experiment, and after 200 h the δ^7Li value of the solution had risen slightly to 10.7‰. Similar results were obtained at pH 11 at 75 °C as can be seen in Fig. 6, with the δ^7Li value of the solution rising to a maximum of 12.2‰.

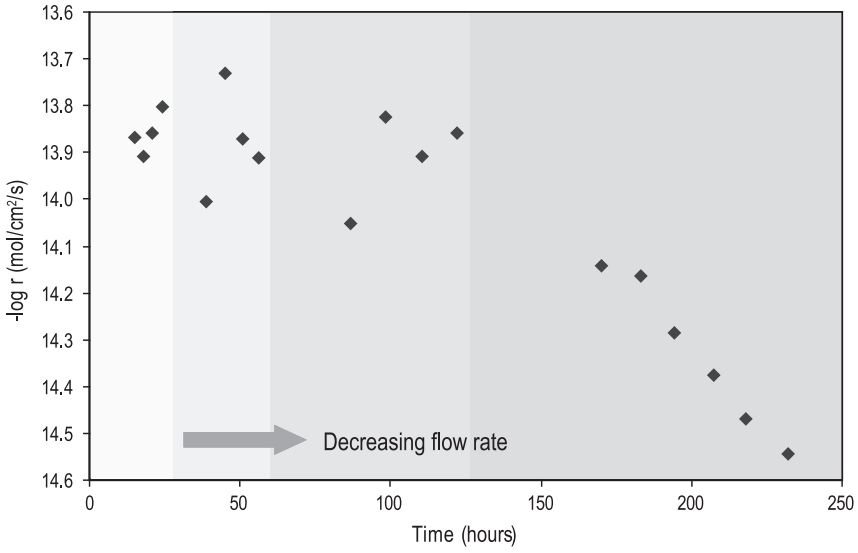

Fig. 4. Dissolution rate of forsterite during the precipitation experiment FO3 (pH 10, 25 °C).

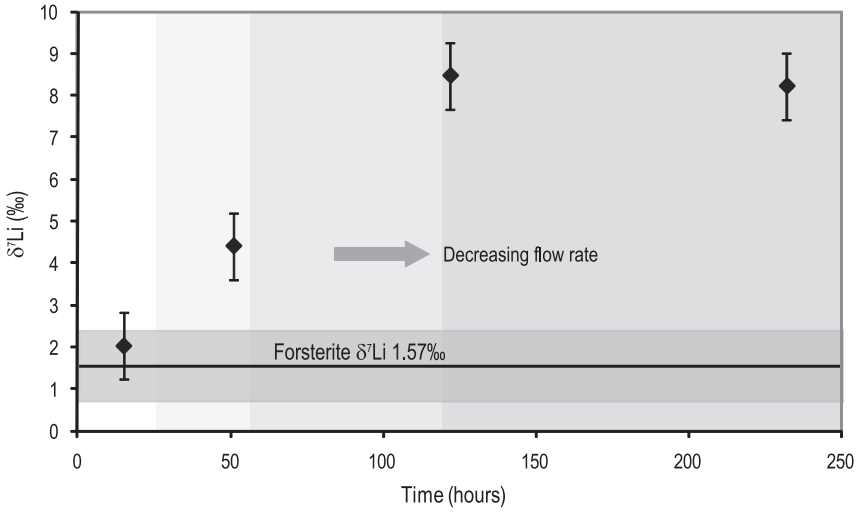

Fig. 5. Lithium isotope composition of experimental fluid during precipitation experiment FO3 (pH 10, 25 °C). Error bars show the external reproducibility (2σ).

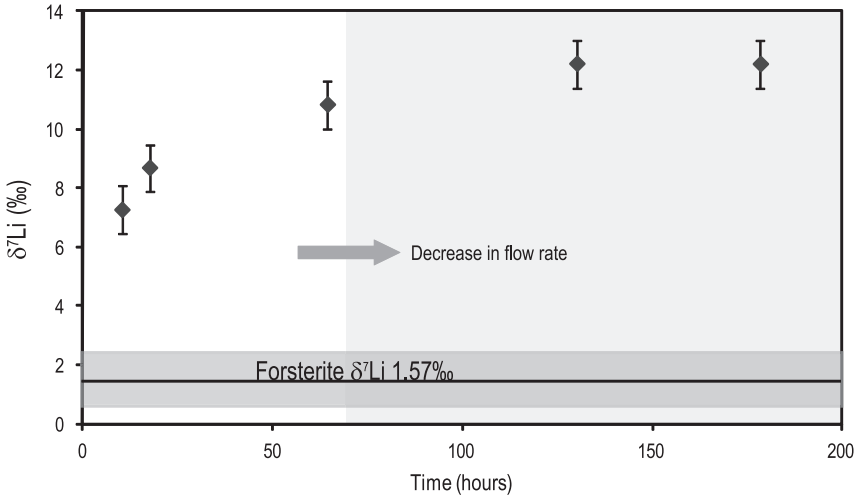

Fig. 6. Lithium isotope ratio of experimental solutions from experiment FO7 (pH 11, 75 °C). Error bars show the external reproducibility (2σ).

In contrast to the Li isotopes, Mg isotope ratios of the experimental solutions are initially always lighter than the dissolving forsterite and with time the solution becomes increasingly heavy. For example at pH 11 and 25 °C (FO5) the δ^{26}Mg composition of the solution evolved from −0.65 to −0.23‰ (Fig. 7). Similarly at 75 °C the δ^{26}Mg value of the solution increased from −0.3‰ to −0.21‰.

4. DISCUSSION

4.1. Dissolution experiments

4.1.1. Stoichiometry

The dissolution rates of basalt glass and forsterite are calculated using Eq. (1). If the dissolution of a mineral is stoichiometric then the elemental ratios in solution are the same as those in the dissolving mineral. Because the dissolution of minerals and glass often involves the formation of precursor complexes, and initially the preferential loss of certain elements, the stoichiometry of the solution can, therefore, be used an indicator of whether the system is at a steady state. If dissolution is non-stoichiometric then the system is unlikely to have reached steady state. In this case the dissolution may involve preferential loss of one or more elements; if this affects the rate of release of Si then the calculated dissolution rate may also be inaccurate. For this reason assessing the stability of the experimental systems is crucial as it may have important implications for the interpretation of the dissolution rates. During the dissolution of basalt glass in low pH solutions there is initially a preferential loss of Al^{3+} into solution (Oelkers and Gislason, 2001). For this reason early experimental solutions should have Si:Al ratios that are lower than the stoichiometric ratio of 2.77 in Stapafell glass (Oelkers and Gislason, 2001). In the case of forsterite, dissolution at low pH causes the initial formation of a Si rich outer layer, thus Mg:Si ratios in the experimental solutions are always higher than the stoichiometric ratio of 1.82 (Pokrovsky and Schott, 2000). During the basalt glass experiments the solutions never attain stoichiometric Si:Al ratios, as can be seen in Tables EA-1 and EA-2. Initially, at 25 °C, the Si:Al ratios of the solutions are below 2.77 and do not become stoichiometric, suggesting that the experiments needed a longer period of time to reach a steady state. Increasing the experimental temperature (to a maximum of 55 °C) caused marked rises in the Si:Al ratio resulting in close to stoichiometric dissolution at pH 4 and 35 °C and pH 3 and 45 °C. At 55 °C the Si:Al ratio is always higher than 2.77. These high Si:Al ratios could be caused by the precipitation of amorphous $Al(OH)_3$ which would remove Al but not Si, thus increasing the Si:Al ratio. However, results of saturation state modelling suggest that amorphous $Al(OH)_3$ was always undersaturated in the experimental solutions (Section 4.1.3). Regardless of the cause, the Si:Al ratios show that the system did not attain a steady state and as such the higher temperature dissolution rates should be interpreted with caution.

In contrast to the dissolution of basalt glass, the fluids produced by forsterite dissolution rapidly attain stoichiometric Mg:Si ratios at pH 2–4. Initially, the Mg:Si ratios of the experimental solutions are slightly higher than stoichiometric, consistent with the preferential release of Mg at low pH (Pokrovsky and Schott, 2000). However, with time this ratio approaches 1.8 and remains at this level for the duration of the experiment, indicating that steady state dissolution has been achieved. On average the Mg:Si ratio was 1.87 ± 0.05 (1σ) over the course of the two experiments and a combined total of 10 days sampling. This is indistinguishable from the average Mg/Si ratio of 1.84 ± 0.19 recorded by Rosso and Rimstidt (2000) during the dissolution of forsterite at low pH.

4.1.2. Dissolution rate

The dissolution rate of basalt glass and forsterite is dependent on temperature and solution composition (Pokrovsky and Schott, 2000; Oelkers and Gislason, 2001) with

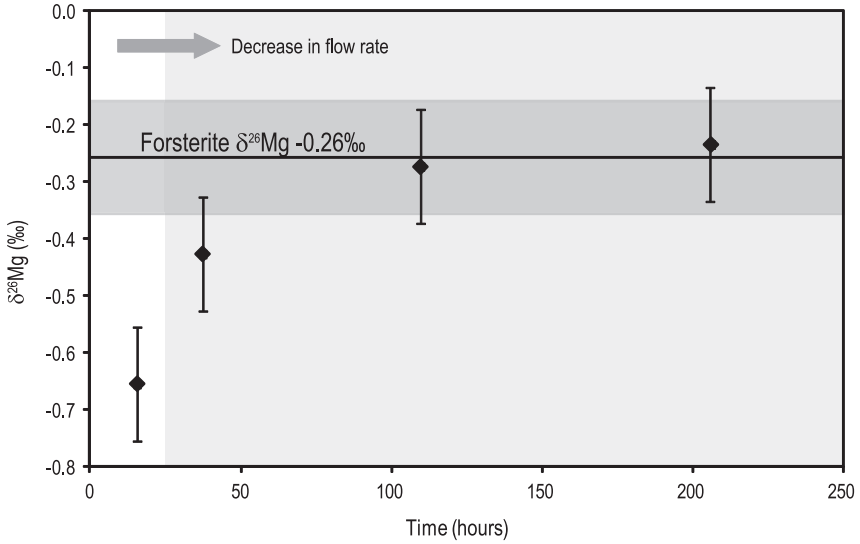

Fig. 7. Magnesium isotope composition of the experimental fluid during dissolution/precipitation experiment FO5 at pH 11 and 25 °C. Error bars show the external reproducibility (2σ).

both increasing temperature and H^+ activity causing dissolution rates to rise, at high undersaturation. Fluid composition affects rates, even at high undersaturation. The H^+ activity (pH) also influences aqueous Al^{3+} speciation which, in turn, affects the basaltic glass dissolution rate (Oelkers and Gislason, 2001). The activity of H^+ decreases faster than the 3rd power of the proton activity when $Al(OH)_4^-$ becomes the dominant Al-species. This occurs at pH greater than about seven depending on the temperature. As a result, basaltic glass dissolution rates increase with increasing pH at alkaline conditions. The increase in dissolution rate with increasing temperature is consistent with the Arrhenius equation. Reactions such as the hydrolysis of silicates increase exponentially with temperature and reaction rates may increase by an order of magnitude by increasing experimental temperatures from 0 to 25 °C (White, 2003). The dissolution mechanisms of both forsterite and basalt glass involve the exchange of protons for metal cations on the mineral surface (Pokrovsky and Schott, 2000; Oelkers and Gislason, 2001). Consequently, the dissolution rate of these materials is more rapid in lower pH solutions where there is a greater concentration of protons. Correspondingly, the composition of the reacted mineral is also more depleted in the low pH experiments; for example at pH 2 the basalt glass lost ~12% of its lithium into solution while at pH 4 the basalt glass lost less than 1%.

Dissolution rates obtained in this study compare very well with previously published data. Despite the dissolution of basalt glass being non-stoichiometric the dissolution rates at pH 2–4 are similar to those obtained by Gislason and Oelkers (2003) as shown in Table 2. This suggests that although steady state dissolution may not have been attained the rate of release of Si has not been significantly affected. The dissolution of forsterite is stoichiometric and correspondingly the dissolution rates of forsterite at pH 2–4 closely match those recorded by Pokrovsky and Schott (2000). While dissolution rates are very similar to those published using stir speeds of 350 rpm, by increasing this rate to over 500 rpm at pH 2 the dissolution rate of both basalt glass and forsterite increases. This effect has been observed before during the dissolution of basalt glass (Gislason and Oelkers, 2003), and attributed to relatively slow diffusional transport of metal ions away from the crystal surface, which limits the dissolution rate at low pH (Gislason and Oelkers, 2003). The increase in stir speed to >500 rpm during the dissolution of forsterite (experiment FO2) caused an increase in the dissolution rate from 2.2×10^{-12} mol/cm^2/s to around 6×10^{-12} mol/cm^2/s. Published dissolution rates for forsterite in pH 2 solutions range from 7×10^{-13} to 2×10^{-12} mol/cm^2/s (Wogelius and Walther, 1991; Pokrovsky and Schott, 2000; Rosso and Rimstidt, 2000). Thus the dissolution rate has increased by nearly three times over that at stir speeds of 350 rpm and by up to one order of magnitude over rates reported previously. These results imply that the dissolution of forsterite is surface reaction controlled, and that stir speeds of 350 rpm are not sufficient to move metal ions away from the dissolving forsterite surface and as a consequence dissolution becomes diffusion limited. While determination of the dissolution rate is not the focus of the current investigation it can be concluded that previous estimates for the dissolution rate of forsterite at low pH and particularly at pH 2 are too low. On this basis it seems likely that the dissolution rate obtained here more accurately reflects that at low pH, and any further studies should take such diffusion processes into account and use a stir speed of at least 500 rpm.

4.1.3. Mineral saturation states

The fact that the dissolution rates in the present study are so similar to those previously determined suggests that the experimental systems were indeed at far from equilibrium conditions as intended. This can be confirmed by modelling the saturation states of primary and secondary minerals in solution using PHREEQC (Parkhurst and Appelo, 1999). This program can calculate the mineral saturation indices of primary and secondary minerals in solution based on element concentrations, temperature and pH. The saturation index is a logarithmic scale indicator of mineral stability: if it is 0 then the mineral is said to be at equilibrium and should be stable in solution. If the SI is >0 then the mineral is said to be supersaturated and may precipitate, and as the SI increases the mineral in question is increasingly likely to precipitate. Minerals and glasses will only precipitate at magmatic temperatures ($T >> 1000$ °C). If the SI is below zero then the mineral is undersaturated, it is unstable in solution and any mineral present will have a tendency to dissolve.

The predictions of mineral stability obtained from PHREEQC are not definitive but they do provide a useful means of estimating mineral stability within the reactors. Equilibrium constants for each mineral were taken from the Wateq4f database (Ball and Nordstrom, 1991) within PHREEQC, data for hydrated basalt glass were taken from Oelkers and Gislason (2001), using a log equilibrium constant of 0.079 at 25 °C for the following hydrolysis reaction:

$$SiAl_{0.36}O_2(OH)_{1.08} + 1.08H^+ \rightarrow SiO_2 + 0.36Al^{3+} + 1.08H_2O \quad (2)$$

The secondary phases that are most likely to form in the reactors are amorphous iron and aluminium hydroxides and/or cryptocrystalline goethite and gibbsite (Gislason and Oelkers, 2003). The results of saturation state modelling show that during the dissolution of basalt glass and forsterite all of these minerals, as well as hydrated basalt glass, kaolinite and illite, are undersaturated and that the degree of undersaturation increases at lower pH. From these results, taken together with solution stoichiometry and dissolution rate data, it is reasonable to assume that the dissolution experiments are all far from equilibrium and that no significant secondary mineral formation has occurred.

4.1.4. Lithium isotope behaviour

As a consequence of the low concentration of Li in the experimental solutions isotope analysis was extremely difficult, and no repeat measurements could be made. The Li isotope composition (δ^7Li) of the basalt glass is ~5.8‰, while the composition of reacted basalt glass ranges from 4.8‰ to 6‰ (Table 2). These values are all within, or close to, the range of Li compositions considered typical for mid ocean ridge basalts (MORB) (Elliott et al., 2006; Tomascak et al.,

2008). The δ^7Li composition for reacted and unreacted forsterite is ~2‰ (Table 2, Fig. 2), similar to the values obtained by Seitz et al. (2004) for San Carlos olivine. In general, the δ^7Li value of the experimental solutions, at low pH, are similar to those of the unreacted starting mineral or glass. The maximum difference in Li isotope composition between reacting solid and the fluid phase was 3‰. This may be caused by compositional heterogeneities in the reacting mineral, the removal or leaching of a surface layer, and/or trace amounts of secondary mineral formation. In the context of the range of Li isotope compositions observed in nature [the recorded range of riverine Li is between 6 and 40‰ (Huh et al., 1998; Pogge von Strandmann et al., 2006)], the small variations in isotope composition observed in these experiments suggest that there is minimal fractionation between mineral and solution at far from equilibrium conditions, consistent with the results of basalt leaching experiments (Pistiner and Henderson, 2003).

4.1.5. Magnesium isotope behaviour

Previously published data indicate a wide range of magnesium isotope compositions for forsterite, even from the same locality. Values of δ^{26}Mg for the San Carlos olivine range from −0.73‰ (Teng et al., 2007), to −0.06‰ (Wiechert and Halliday, 2007). This range of 0.7‰ is significant, given that the range of Mg isotope ratios for silicate rocks is between 0‰ and −1‰ (Young and Galy, 2004; Tipper et al., 2006a). It has been proposed that these differences reflect heterogeneity of the San Carlos olivine (Pearson et al., 2006) or variations caused by weathering or metasomatic affects (Teng et al., 2007). However, analytical artefacts associated with the chemical separation of Mg or analytical procedures may also be an issue. The Mg isotope composition of San Carlos forsterite measured in this study, shown in Fig. 3 and Table 4, falls within the reported range with a δ^{26}Mg value of −0.26‰, similar to the value obtained recently using a standard addition technique (Tipper et al., 2008). The isotope compositions of the reacted forsterite are similar to that of the unaltered starting material (δ^{26}Mg = −0.31 and −0.34‰). Although the Mg isotope ratios are slightly lighter, they are within the analytical uncertainty of the value obtained for unaltered forsterite.

Basalt has also been widely analysed for Mg isotopes; for example the δ^{26}Mg composition of SUNY MORB ranges between −0.28 and −0.32‰ (Teng et al., 2007; Richter et al., 2008) while the composition of BCR-1 ranges from −0.37 (Young and Galy, 2004) to −0.09‰ (Wiechert and Halliday, 2007). The Stapafell basaltic glass, analysed here, has a very similar Mg composition to these basalts with a δ^{26}Mg of −0.3‰ (Table 4). The composition of the reacted basalt glass is very similar, suggesting that the sample is homogeneous and that there has been no measurable fractionation during dissolution.

Relative to the reacting basalt glass or forsterite the experimental fluid always has a light δ^{26}Mg isotope composition as shown in Fig. 3 and Table 4. Furthermore, the Mg isotope ratio of that fluid always becomes lighter with time. For the Mg isotope ratio of the fluid and reacting mineral/glass to be different there either needs to be fractionation during the dissolution process (i.e. one isotope is preferentially lost into solution) or preferential incorporation of one isotope during secondary mineral formation. Weathering studies have shown that heavy Mg is preferentially retained in silicate soils, specifically attributed to incorporation into smectite (Tipper et al., 2006a). However, saturation state modelling and solution stoichiometry suggest that there has been little or no formation of secondary minerals. For example, during the dissolution of forsterite the Mg:Si ratio is always stoichiometric. If secondary silicate mineral formation had occurred it might be expected that Si would be removed from solution, causing the Mg:Si ratio to change. Similarly if iron oxides had formed the Mg:Fe ratio of the solution would change, whereas it is always ~10.5 implying that there has been no iron mineral precipitation.

If secondary minerals have not formed then the alternative is that there has been preferential loss of light Mg during the dissolution of basalt glass and forsterite. A similar process is thought to operate for Si isotopes during the dissolution of basalt glass (Ziegler et al., 2005); experimental data indicate that the fluid phase is initially enriched in the light isotope of Si (^{28}Si) possibly because of a higher abundance of ^{28}Si on mineral surfaces. Mass balance then requires that at some point during dissolution heavy Si (or in the present study, heavy Mg) must be preferentially released into solution so that the final composition of the solution matches that of the dissolving mineral or glass. If this process were shown to operate then this would have significant implications for our interpretation of the behaviour of Mg in natural systems.

4.2. Dissolution/precipitation experiments at high pH

4.2.1. Stoichiometry

Unlike the forsterite dissolution experiments where stoichiometric dissolution was rapidly attained, the composition of the fluid from the dissolution–precipitation experiments indicates that stoichiometric dissolution did not occur. This is illustrated in Fig. 8a where the Mg:Si ratio for FO3 at pH 10 is shown against time. Initially the ratio is always lower than 1.8 because in high pH solutions the dissolution mechanism involves the formation of a Mg rich layer at the forsterite surface, resulting in a low Mg concentration in the aqueous solution (Pokrovsky and Schott, 2000). With time the Si and Mg concentrations in solution increase as the flow rates are decreased, this is accompanied by an increase in the Mg:Si ratio as shown in Fig. 8a and Table EA-3. This change in the solution chemistry indicates that the system is moving towards a steady state. However when the flow rate of the solution is reduced further, to 0.15 g/min there is a change in the trend. Instead of a continuing Mg:Si ratio increase towards 1.8, the ratio drops, as does the concentration of Mg and Si. This suggests that some process is removing both Mg and Si from solution, and the most likely explanation is that secondary minerals are forming. Because both Mg and Si are removed from solution it is likely that any secondary phase is a magnesium silicate. Moreover, because the Mg:Si ratio is decreasing in the solution the stoichiometric ratio of Mg:Si in the new mineral must be >1. In this case the most likely mineral to have formed is chrysotile, which has the formula $Mg_3(Si_2O_5)(OH)_4$.

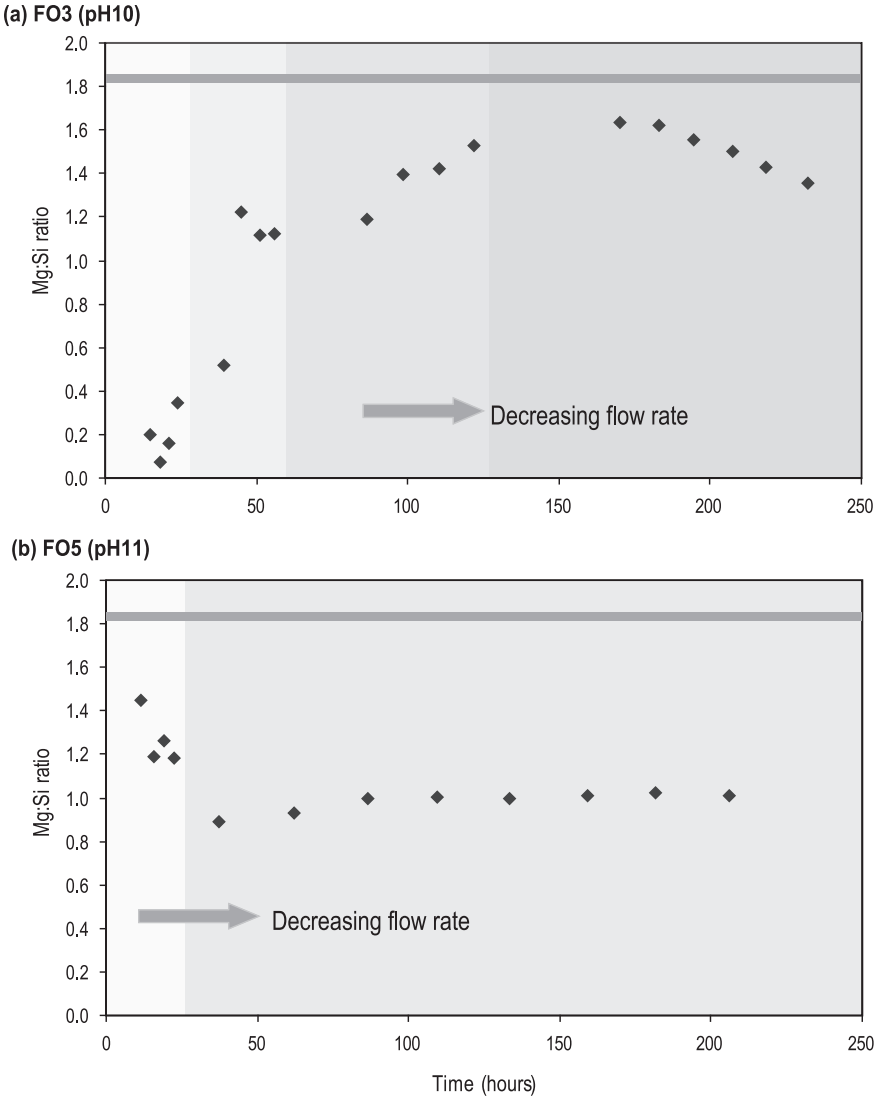

Fig. 8. Mg:Si ratios of experimental solutions from (a) experiment FO3 at pH 10, and 25 °C and (b) experiment FO5 at pH 11. Both experiments were conducted at 25 °C.

If the solutions in Fig. 8, from the pH 10 and 11 forsterite experiments, are compared it is clear that those at pH 10 have Mg:Si ratios that are closer to the stoichimetric ratio than those from the pH 11 experiments. At pH 10 Mg:Si ratios are ~1.5 and at pH 11 Mg:Si ratios are ~1.1. That stoichiometric dissolution is not attained could be due to the lower dissolution rate at high pH (Wogelius and Walther, 1991; Pokrovsky and Schott, 2000). High pH experiments involving the dissolution of forsterite are known to take at least 200–300 h to reach a steady state (Pokrovsky and Schott, 2000). Nevertheless, even though all high pH experiments in this study were run for a minimum of 200 h the solutions did not approach stoichiometric Mg:Si ratios, rather it seems likely that secondary mineral formation has altered the solution composition in all experiments.

4.2.2. Mineral saturation states

Evidence from solution stoichiometry and concentration data suggests that secondary mineral formation has occurred during these experiments, and saturation state modelling can help to confirm this. High pH solutions promote the formation of secondary minerals because the concentration of protons in solution is much lower. The relatively simple composition of forsterite means that only a limited number of secondary minerals that can form. Because forsterite contains little Al the formation of clays cannot occur, and although Fe is present, even in the forsterite rich olivine, the concentrations in the aqueous solution are below the detection limits of ICP-AES so it can be assumed that the formation of Fe-oxyhydroxides is also not significant. Carbonate precipitation is more likely because CO_2 solubility is high at high pH and carbonate CO_3^{2-} is the main carbon species at pH >10.3 [e.g. (Appelo and Postma, 2005)]. However the input solution was encased in a mantle of nitrogen gas, making the formation of carbonates unlikely. Taken together with evidence given in Section 4.2.1, these observations suggest that the most likely minerals to form are Mg-silicates such as chrysotile. Saturation state

modelling of the experimental solutions show that at pH 10 and 11 and 25 °C the solutions were supersaturated with respect to both chrysotile and talc, so in theory one or both of these minerals could have precipitated, as is illustrated in Fig. 9.

At higher temperature (75 °C) the solutions are slightly less saturated with respect to secondary minerals. This is because at higher temperature the pH of a solution will change, for example, a solution that has a pH of ~10 at 25 °C will have an *in situ* pH of ~9 at 75 °C. This is because of the temperature dependence of the dissociation constants of the weak acids in solution. As has already been outlined the stability of silicate minerals is highly dependent on the pH of the solution. The stability of magnesium silicate minerals increases as the pH of the solution rises and vice versa. Nevertheless, all solutions at 75 °C are oversaturated with respect to chrysotile and many are oversaturated with respect to talc.

At higher saturation states there is an increasing likelihood that secondary minerals will form, but the rate of forsterite dissolution is also affected. Although forsterite is undersaturated in all experiments the solutions are far closer to equilibrium at high pH as shown in Fig. 9. The saturation index (SI) for forsterite was around -30 at pH 2 to 4 (FO2). In comparison at pH 11 (experiment FO7), the saturation index of forsterite was around -2. When a mineral approaches equilibrium the dissolution rate no longer simply reflects forward dissolution but is also influenced by the reverse reaction (Gislason and Oelkers, 2003) in which case the rate of dissolution may decrease. This inhibition of the dissolution rate can be quantified by calculating the Gibbs free energy of the reaction (ΔG_r):

$$\Delta G_r = \frac{R \times T \times 2.303 \times SI}{1000} \quad (3)$$

where R is the gas constant, T is the temperature in K and 2.303 is the natural log–decimal log conversion factor .

A dissolution reaction will become dependent on the saturation state of the reactants at ΔG_r values of 0 to −10 kJ/mol for basalt glass and ΔG_r values of 0 to −20 kJ/mol for forsterite (Flaathen and Gislason, 2007). The braking effect of saturation state on the dissolution rate can be quantified using the following simplified equation to calculate the affinity term:

$$\text{Affinity term} = (1 - \exp^{\left[\frac{\Delta G_r}{\sigma RT}\right]}) \quad (4)$$

where ΔG_r is the Gibbs free energy of reaction, R is the gas constant and T is the temperature (K).

σ is Temkins stoichiometric constant and is the ratio of the mineral stoichiometry and the stoichiometry of the activated complex (Oelkers, 2001b). For basalt glass this value is 1, for forsterite this value is 2.

Eq. (4) applies to multi-oxides where the chemical formula has been normalised to the formation of one rate-controlling precursor complex (Oelkers, 2001b). In experiment FO3 (pH 10, 25 °C) the ΔG_r of forsterite changes from around −50 to −15 kJ/mol. The increasing solution concentrations cause the dissolution of forsterite to change from being saturation state independent to saturation state dependent, resulting in a slowdown of the dissolution rate by ~5%. In experiment FO5 (pH 11, 25 °C) forsterite is more stable because the pH is higher, and the dissolution of forsterite is slowed by between 3% and 13%.

At 75 °C the equilibrium constant (K_{eq}) for forsterite changes as shown below in Eq. (5):

$$K_{\text{forsterite}} = 2\log\left(\frac{a_{Mg^{2+}}}{a^2_{H+}}\right) + \log a_{H_2SiO_4} = 28.29 \text{ at } 25\,^\circ\text{C}$$
$$= 23.19 \text{ at } 75\,^\circ\text{C} \quad (5)$$

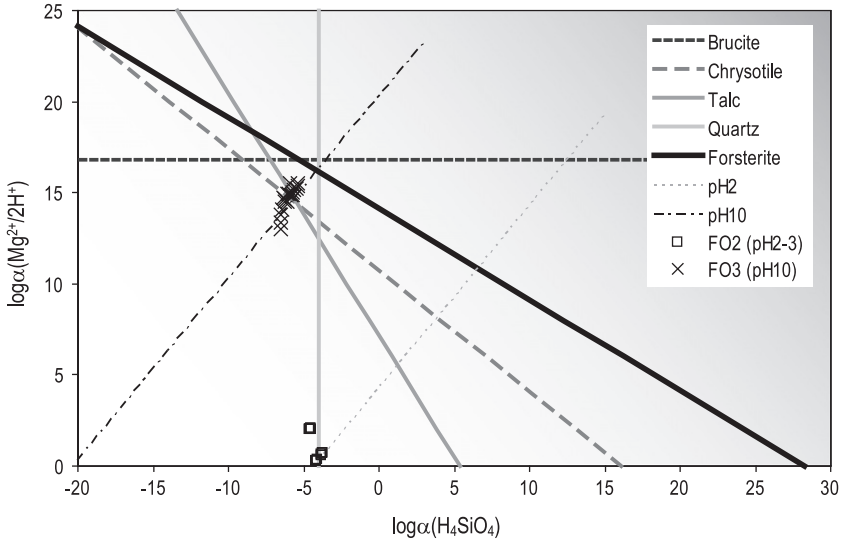

Fig. 9. A magnesium silicate stability diagram showing the saturation state of experimental solutions from experiment FO2 (pH 2–3, 25 °C) and experiment FO3 (pH 10, 25 °C). At pH2 the experimental solutions are far from equilibrium with respect to Mg-silicates. In contrast at pH 10 the experimental solutions are oversaturated with respect to chrysotile and talc. The equilibrium constants are from the Wateq4f database (Ball and Nordstrom, 1991).

Because the equilibrium constant changes, a solution with a given activity of Mg^{2+} and pH will be closer to equilibrium at 75 °C than at 25 °C. However because pH decreases at higher temperatures the result is that the dissolution rate of forsterite falls by between 5% and 22%, comparable with the effect of saturation state at 25 °C.

In summary, the evidence from elemental ratios and mineral saturation states suggests that secondary mineral formation has occurred. Relatively high saturation indices for forsterite suggest that the dissolution rate has been inhibited. Taken together this suggests that calculated dissolution rates at high pH must be lower than those obtained at far from equilibrium conditions.

4.2.3. Dissolution rates

As outlined in Section 4.2.2, the dissolution rates calculated from dissolved Si concentrations, at a slow flow rate and high pH, cannot be regarded as representative of those of far from equilibrium dissolution. The removal of Si from solution by secondary minerals and the inhibiting effect of the high forsterite saturation (Eq. (4)) results in dissolution rates that are lower than those at far from equilibrium conditions. Nevertheless, the dissolution rate data can provide useful information. For the forsterite experiments performed at pH 10 and 11, FO3 and FO5, the apparent dissolution rate changed as the flow rate decreased. For example, in FO3 the dissolution rate was a relatively constant 1.3×10^{-14} mol/cm^2/s over the first 130 h when the flow rate was always >1 (Fig. 4). Only at a flow rate of 0.15 g/min do both Mg and Si start to be removed from solution and the apparent dissolution rate falls to 3.2×10^{-15} mol/cm^2/s. The decrease in flow rate causes an initial build up of concentration in solution, and increasing saturation states. Thus, the decreasing Mg and Si concentrations coincide with an increasing likelihood of secondary mineral formation and resulting values of r cannot be considered as reliable. For this reason the value of r over the first 130 h is the most accurate estimate of the dissolution rate. While stoichiometric dissolution may not have been attained during this period the dissolution rate is relatively stable, and it is unlikely that there would have been a significant change in r with time. Similarly, at pH 11 the apparent dissolution rate is heavily dependent on the flow rate. A reduction in the flow rate from 3 to 0.2 g/min results in a decline in the dissolution rate of forsterite to $\sim 3.2 \times 10^{-15}$ mol/cm^2/s (Table EA-3), similar to that seen at pH 10 and comparable to the dissolution rates obtained by Pokrovsky and Schott (2000) (Fig. 10). While changes in the dissolution rate could be caused by the system establishing equilibrium, the Mg:Si ratios would be expected to become stoichiometric when in fact they become less so. Again it is likely that the decrease in dissolution rate is associated with secondary mineral formation.

The results suggest that forsterite dissolution in pH 10–11 solutions is faster than the value of 3.2×10^{-15} mol/cm^2/s reported in Pokrovsky and Schott (2000), in addition the dissolution rate of forsterite at pH 11 may be faster than it is at pH 10, consistent with the data of Wogelius and Walther (1991). However, definitive conclusions cannot be drawn because the aim of the dissolution–precipitation experiments here was not to calculate far from equilibrium dissolution rates, and while the dissolution rates are faster at higher flow rates (1–4 g/min) steady state dissolution was not achieved. In order to confirm how the dissolution rate of forsterite behaves in high pH solutions further experiments are needed at high flow rates and for a longer duration (i.e. a minimum of 200 h).

4.2.4. Secondary phase identification

The combined evidence from solution chemistry, saturation state modelling and dissolution rates suggest that dissolution of forsterite at conditions close to equilibrium resulted in the formation of secondary minerals. Because Li and Mg isotopes are sensitive to secondary mineral formation it is important to be able to unambiguously confirm whether secondary mineral formation has occurred or not,

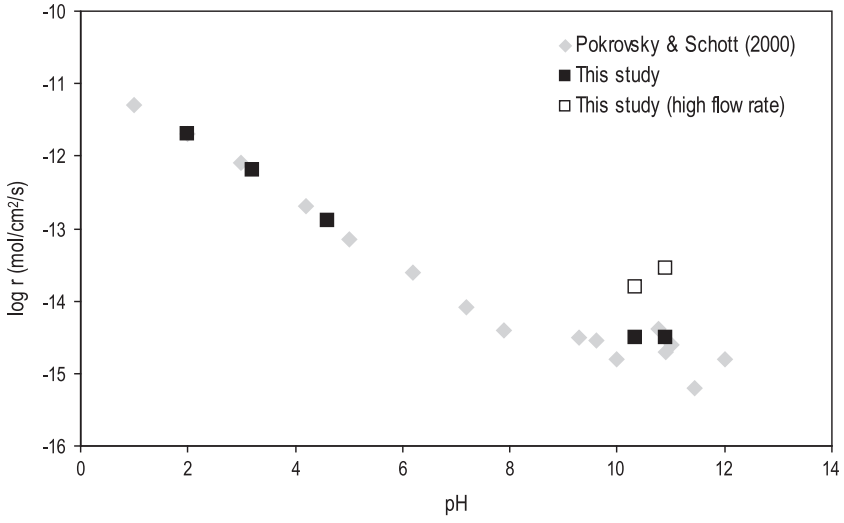

Fig. 10. Comparison of forsterite dissolution rates obtained in this study (at 25 °C, and a constant stir speed) with those published by Pokrovsky and Schott (2000).

and if possible to identify the secondary phase. A preliminary SEM investigation of the solid phases from FO3, FO6 and FO7 was unable to find any evidence of secondary mineral formation, probably because the mass of secondary mineral formed was very low. However these reacted phases were also analysed by XRD, the results of which confirm the results of saturation state modelling that chrysotile is present, and is the principal secondary phase produced in these experiments. While saturation state modelling also suggested that talc and brucite could have formed, the XRD analyses cannot confirm the presence of these phases in any of the experiments.

4.2.5. Lithium isotope behaviour

During the dissolution–precipitation experiments the Li isotope composition of the solutions became increasingly heavy as shown in Figs. 5 and 6. This behaviour contrasts with that of the dissolution experiments (Fig. 2 and Table 2) where the Li isotope compositions of the solutions remained relatively constant and similar to that of the dissolving forsterite ($\delta^7Li \approx 2‰$). That the solutions are isotopically heavy suggests that ^7Li is preferentially lost into solution, consistent with previous work on weathering in natural waters (Chan et al., 1992; Huh et al., 1998; Seyfried et al., 1998; Pistiner and Henderson, 2003; Kisakurek et al., 2005). The simplest way to enrich the fluid phase in ^7Li is by incongruent loss of Li isotopes during mineral dissolution. However this hypothesis can be discounted for two reasons; (a) the isotopic composition of the fluid in the dissolution experiments is similar to the composition of the dissolving mineral, and (b) the mineral phase at the end of the experiments has a δ^7Li composition that is indistinguishable from that of an unaltered sample (Table 2).

Instead, the weight of evidence from analyses of the experimental solutions and from XRD analyses of the reacted phases suggests that secondary mineral formation has occurred with the principal secondary phase being chrysotile. The light ^6Li isotope has been preferentially removed from solution and incorporated into chrysotile during its formation, enriching the residual fluid in the heavy ^7Li isotope. This behaviour is consistent with both experimental and natural studies of Li isotopes and is supported by the positive relationship between chrysotile saturation state and the δ^7Li isotope composition of the fluid (Fig. 11). While XRD could identify the presence of chrysotile, it could not be found during SEM analysis probably because the mass of chrysotile that has precipitated is likely to be very low. In this regard, the change in solution chemistry during experiment FO3 can be used to predict just how much chrysotile may have formed by using the change in dissolution rate (Fig. 4) to quantify the amount of Si removed from solution. For this experiment the amount of Si that has been removed is ~0.14 mg which equates to ~0.7 mg of chrysotile which is just ~0.007% of the total mass of forsterite in the reactor (10 g), and would be difficult to find. This observation highlights the sensitivity of the Li isotope composition in aquatic solutions to even the smallest amount of secondary mineral formation.

4.2.6. Magnesium isotope behaviour

At far from equilibrium conditions, the dissolution of forsterite results in the experimental solution having a light $\delta^{26}Mg$ isotope composition relative to unaltered forsterite. During the dissolution–precipitation experiments the solution initially shifts to light $\delta^{26}Mg$ isotope compositions. However as the experiments proceed and the solutions become more saturated with respect to secondary minerals the $\delta^{26}Mg$ composition of the solution becomes heavier and continues to do so until the end of the experiment. The combined evidence presented in Section 4.2 suggests that chrysotile is the principal secondary phase formed during the precipitation experiments. Previous investigations suggest the isotopic behaviour of magnesium is mineral specific and differs between carbonates and silicates (Galy et al., 2002; Tipper et al., 2006a). If the assumption that magnesium silicates have formed is correct then the results

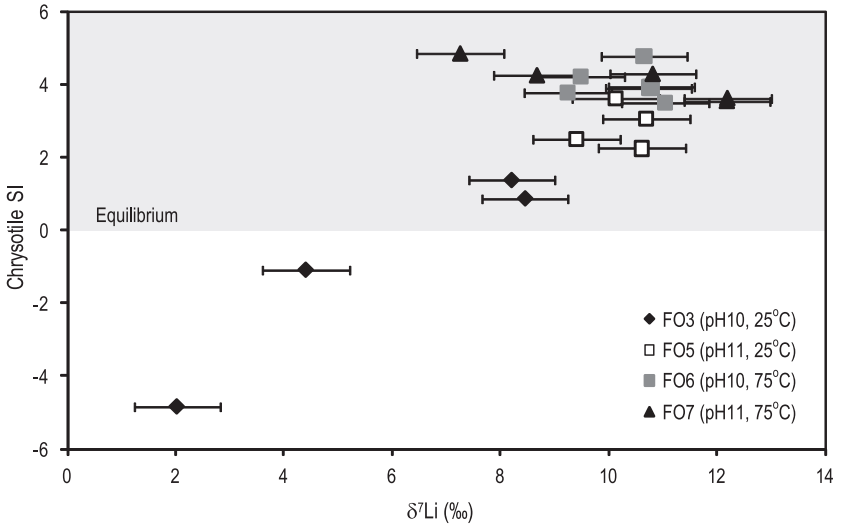

Fig. 11. A graph showing the δ^7Li (‰) values of solutions from the precipitation experiments plotted vs the saturation state of chrysotile. Error bars show the external reproducibility (2σ).

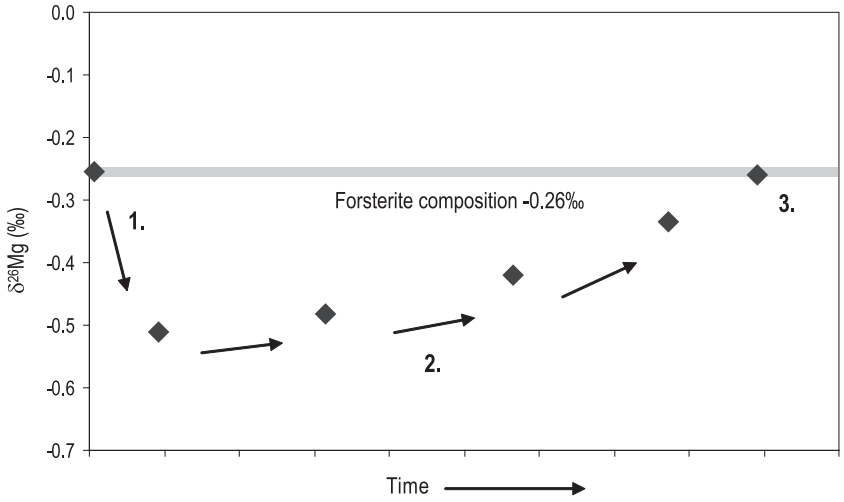

Fig. 12. A diagram showing the theoretical evolution of the magnesium isotopic composition of the dissolved phase during the dissolution of a mineral grain at far from equilibrium. The fluid develops light Mg isotope ratios relative to the dissolving forsterite as it begins to dissolve, as inferred from results of the dissolution experiments (1). As the mineral continues to dissolve mass balance requires the solution to become isotopically heavier (2) and eventually as the entire mineral dissolves the composition of the fluid will match that of the dissolving mineral (3).

of this study suggest that phases such as chrysotile preferentially incorporate the light isotopes of magnesium during their formation leaving a solution with a relatively heavy Mg isotope composition.

One alternative that might explain the behaviour of Mg in supersaturated solutions is linked to the process of dissolution. During straightforward dissolution of forsterite the solution became isotopically light, but mass balance dictates that this cannot continue indefinitely. If a mineral is to dissolve totally then the solution must have the same isotopic composition as the dissolving mineral. Therefore if forsterite dissolution initially involves the preferential loss of light magnesium in solution then at some point during the dissolution process there must be loss of heavy magnesium (Fig. 12). While this, in theory, could explain the results of the dissolution–precipitation experiments it should be remembered that despite the high pH experiments running for longer, the dissolution rate at pH 10 and 11 is around two orders of magnitude slower than at pH 2–4. For this reason the total amount of forsterite dissolved at high pH should be lower than in the dissolution experiments at low pH. Because the fluid composition in the dissolution experiments did not become isotopically heavy at any stage (e.g. Fig. 3) it is unreasonable to suggest that a mass balance effect is only occurring in the precipitation experiments. Therefore, the overwhelming evidence suggests that the shift to heavier Mg isotopes in the experimental fluid is a result of secondary mineral formation.

If these results are applied to the oceanic Mg budget then the relatively heavy Mg isotope ratio in seawater could result from Mg uptake into silicate minerals during weathering. Magnesium is removed from seawater when hydrothermal fluid interacts with the crust, forming smectites and at higher temperatures chlorite (German and Von Damm, 2003). The off axis removal of Mg at ridge flanks can potentially account for a significant proportion of the Mg input from rivers (Elderfield and Schultz, 1996). While it is currently unclear whether the oceans are at a steady state with respect to Mg (Holland, 2005) our results suggest that the uptake of Mg into secondary silicates should be considered as a possible control over the δ^{26}Mg value of seawater.

5. CONCLUSIONS

The results of these laboratory experiments have implications for the interpretation of Li and Mg isotope data in natural waters. We have demonstrated that forsterite dissolves congruently with respect to Li isotopes, and we have confirmed that this is also true for dissolution of basalt glass. However, our experimental data show that Li isotopes are fractionated during the formation of chrysotile, with preferential uptake of ^{7}Li into this secondary mineral phase. This is consistent with field studies of river waters, which demonstrate that the Li isotopic composition of the suspended and bed sediments is always isotopically lighter than that of the corresponding dissolved phase.

Our results for Mg indicate that the behaviour of Mg isotopes during weathering is more complicated. During dissolution of forsterite, the light isotope of Mg is preferentially incorporated into the dissolved phase. Precipitation of chrysotile preferentially removes light Mg from solution, so the dissolved phase becomes increasingly enriched in heavy Mg over time. Other studies have shown that precipitation of carbonates also preferentially removes light Mg from solution, whereas the formation of clay minerals in silicate soils appears to preferentially incorporate heavy Mg isotopes in preference to the lighter isotopes. Removal of isotopically light Mg from solution during secondary mineral formation could help to explain why the Mg isotope ratio of seawater is heavier than that of the average riverine Mg flux. Nevertheless, our data indicate that the interpretation of Mg isotope variations in natural systems is challenging, and further studies of the behaviour of Mg isotopes during weathering of different mineral phases in both the

laboratory and the field are required to better understand and quantify the behaviour of the Mg isotope system.

ACKNOWLEDGMENTS

We are grateful for the help of many people who assisted during the course of this project. Specific thanks to Bergur Sigfusson, Eydis Eiriksdottir and Ingvi Gunnarsson at the University of Iceland for their help with running the dissolution experiments. Thanks also to Sam Hammond and Nick Rogers for help with ICP-MS analyses at The Open University. We would also like to extend our thanks to Anne Iserentant and Sophie Opfergelt (from the Environmental Sciences – Soil Science department, Earth and Life Institute, Université Catholique de Louvain, Belgium) for help with XRD identification of secondary phases. Finally, we would like to thank Jerome Gaillardet, Paul Tomascak and one anonymous reviewer for their helpful comments which have greatly improved this manuscript. This work was supported by a PhD studentship to J.W. funded by the UK Natural Environment Research Council (NE/B502701/1). PPvS and the Bristol work was supported by NERC grant NER/C510983/1.

APPENDIX A. SUPPLEMENTARY DATA

Supplementary data associated with this article can be found, in the online version, at doi:10.1016/j.gca.2010.06.028.

REFERENCES

Appelo C. A. J. and Postma D. (2005) *Geochemistry, groundwater and pollution*. A.A. Balkema.

Ball J. W. and Nordstrom D. K. (1991) User's manual for WATEQ4F, with revised thermodynamic data base and text cases for calculating speciation of major, trace, and redox elements in natural waters, pp. 193.

Berger G., Claparols C., Guy C. and Daux V. (1994) Dissolution rate of a basalt glass in silica-rich solutions – implications for long-term alteration. *Geochim. Cosmochim. Acta* **58**(22), 4875–4886.

Berger G., Schott J. and Guy C. (1988) Behavior of Li, Rb and Cs during basalt glass and olivine dissolution and chlorite, smectite and zeolite precipitation from seawater – experimental investigations and modelization between 50 and 300 °C. *Chem. Geol.* **71**(4), 297–312.

Berner R. A. (2004) A model for calcium, magnesium and sulfate in seawater over Phanerozoic time. *Am. J. Sci.* **304**(5), 438–453.

Bi E. B. B., Poszwa A., and Vigier N. (2008) Experimental determination of magnesium isotope fractionation during higher plant growth. *Geophysical Research Abstracts* 10(EGU 2008).

Black J. R., Yin Q.-z. and Casey W. H. (2006) An experimental study of magnesium-isotope fractionation in chlorophyll-a photosynthesis. *Geochim. Cosmochim. Acta* **70**(16), 4072–4079.

Brantley S. L. (2003) Reaction kinetics of primary rock-forming minerals under ambient conditions. In *Treatise on Geochemistry* (eds. H. D. Holland and K. K. Turekian). Pergamon, pp. 73–117.

Brantley S. L. and Stillings L. (1996) Feldspar dissolution at 25 °C and low pH. *Am. J. Sci.* **296**(2), 101–127.

Brunauer S., Emmett P. H. and Teller E. (1938) Adsorption of gases in multimolecular layers. *J. Am. Chem. Soc.* **60**(2), 309–319.

Chan L. H. and Edmond J. M. (1988) Variation of lithium isotope composition in the marine-environment – a preliminary-report. *Geochim. Cosmochim. Acta* **52**(6), 1711–1717.

Chan L. H., Edmond J. M. and Thompson G. (1993) A lithium isotope study of hot-springs and metabasalts from midocean ridge hydrothermal systems. *J. Geophys. Res. Solid Earth* **98**(B6), 9653–9659.

Chan L. H., Edmond J. M., Thompson G. and Gillis K. (1992) Lithium isotopic composition of submarine basalts – implications for the lithium cycle in the oceans. *Earth Planet. Sci. Lett.* **108**(1–3), 151–160.

Chan L. H., Gieskes J. M., You C. F. and Edmond J. M. (1994) Lithium isotope geochemistry of sediments and hydrothermal fluids of the Guaymas Basin, Gulf of California. *Geochim. Cosmochim. Acta* **58**(20), 4443–4454.

Chan L. H. and Hein J. R. (2007) Lithium contents and isotopic compositions of ferromanganese deposits from the global ocean. *Deep-Sea Res. II Top. Stud. Oceanogr.* **54**(11–13), 1147–1162.

Chang V. T. C., Williams R. J. P., Makishima A., Belshawl N. S. and O'Nions R. K. (2004) Mg and Ca isotope fractionation during $CaCO_3$ biomineralisation. *Biochem. Biophys. Res. Commun.* **323**(1), 79–85.

Chen Y. and Brantley S. L. (2000) Dissolution of forsteritic olivine at 65 °C and $2 > pH < 5$. *Chem. Geol.* **165**(3–4), 267–281.

Crovisier J. L., Honnorez J. and Eberhart J. P. (1987) Dissolution of basaltic glass in seawater – mechanism and rate. *Geochim. Cosmochim. Acta* **51**(11), 2977–2990.

Crovisier J. L., Thomassin J. H., Juteau T., Eberhart J. P., Touray J. C. and Baillif P. (1983) Experimental seawater basaltic glass interaction at 50 °C – study of early developed phases by electron-microscopy and X-ray photoelectron spectrometry. *Geochim. Cosmochim. Acta* **47**(3), 377–387.

Daux V., Guy C., Advocat T., Crovisier J. L. and Stille P. (1997) Kinetic aspects of basaltic glass dissolution at 90 °C: role of aqueous silicon and aluminium. *Chem. Geol.* **142**(1–2), 109–126.

de Villiers S., Dickson J. A. D. and Ellam R. M. (2005) The composition of the continental river weathering flux deduced from seawater Mg isotopes. *Chem. Geol.* **216**(1–2), 133–142.

Depaolo D. J. and Ingram B. L. (1985) High-resolution stratigraphy with strontium isotopes. *Science* **227**(4689), 938–941.

Devidal J., Schott J. and Dandurand J. (1997) An experimental study of kaolinite dissolution and precipitation kinetics as a function of chemical affinity and solution composition at 150 °C, 40 bars, and pH 2, 6.8, and 7.8. *Geochim. Cosmochim. Acta* **61**(24), 5165–5186.

Elderfield H. and Schultz A. (1996) Mid-ocean ridge hydrothermal fluxes and the chemical composition of the ocean. *Annu. Rev. Earth Planet. Sci.* **24**(1), 191–224.

Elliott T., Thomas A., Jeffcoate A. and Niu Y. (2006) Lithium isotope evidence for subduction-enriched mantle in the source of mid-ocean-ridge basalts. *Nature* **443**(7111), 565–568.

Flaathen T. K. and Gislason S. R. (2007) The effect of volcanic eruptions on the chemistry of surface waters: The 1991 and 2000 eruptions of Mt. Hekla, Iceland. *J. Volcanol. Geothermal Res.* **164**(4), 293–316.

Galy A., Bar-Matthews M., Halicz L. and O'Nions R. K. (2002) Mg isotopic composition of carbonate: insight from speleothem formation. *Earth Planet. Sci. Lett.* **201**(1), 105–115.

GERM (2000) Geochemical Earth Reference Model. Available from: www.Earthref.org.

German C. and Von Damm K. (2003) Hydrothermal processes. *Treatise Geochem.* **6**, 181–222.

Gislason S. R. and Oelkers E. H. (2003) Mechanism, rates, and consequences of basaltic glass dissolution: II. An experimental study of the dissolution rates of basaltic glass as a function of pH and temperature. *Geochim. Cosmochim. Acta* **67**(20), 3817–3832.

Handler M., Baker J., Schiller M., Bennett V. and Yaxley G. (2009) Magnesium stable isotope composition of Earth's upper mantle. *Earth Planet. Sci. Lett.* **282**(1–4), 306–313.

Harder H. (1972) The role of magnesium in the formation of smectite minerals. *Chem. Geol.* **10**(1), 31–39.

Hess J., Bender M. L. and Schilling J. G. (1986) Evolution of the ratio of Sr-87 to Sr-86 in seawater from Cretaceous to present. *Science* **231**(4741), 979–984.

Holland H. D. (2005) Sea level, sediments and the composition of seawater. *Am. J. Sci.* **305**(3), 220–239.

Huh Y., Chan L. H., Zhang L. and Edmond J. M. (1998) Lithium and its isotopes in major world rivers: implications for weathering and the oceanic budget. *Geochim. Cosmochim. Acta* **62**(12), 2039–2051.

James R. H. and Palmer M. R. (2000) The lithium isotope composition of international rock standards. *Chem. Geol.* **166**(3–4), 319–326.

Jeffcoate A., Elliott T., Thomas A. and Bouman C. (2004) Precise/Small Sample Size Determinations of Lithium Isotopic Compositions of Geological Reference Materials and Modern Seawater by MC-ICP-MS. *Geostand. Geoanal. Res.* **28**(1), 161–172.

Jeffcoate A. B., Elliott T., Kasemann S. A., Ionov D., Cooper K. and Brooker R. (2007) Li isotope fractionation in peridotites and mafic melts. *Geochim. Cosmochim. Acta* **71**(1), 202–218.

Kisakurek B., James R. H. and Harris N. B. W. (2005) Li and δ^7Li in Himalayan rivers: proxies for silicate weathering? *Earth Planet. Sci. Lett.* **237**(3–4), 387–401.

Liu Y., Olsen A. A. and Rimstidt J. D. (2006) Mechanism for the dissolution of olivine series minerals in acidic solutions. *Am. Mineral.* **91**(2–3), 455–458.

Marschall H. R., Pogge von Strandmann P. A. E., Seitz H.-M., Elliott T. and Niu Y. (2007) The lithium isotopic composition of orogenic eclogites and deep subducted slabs. *Earth Planet. Sci. Lett.* **262**(3–4), 563–580.

Millot R., Guerrot C. and Vigier N. (2007) Accurate and high-precision measurement of lithium isotopes in two reference materials by MC-ICP-MS. *Geostand. Geoanal. Res.* **28**(1), 153–159.

Murphy W. M. and Helgeson H. C. (1989) Thermodynamic and kinetic constraints on reaction-rates among minerals and aqueous-solutions 4. Retrieval of rate constants and activation parameters for the hydrolysis of pyroxene, wollastonite, olivine, andalusite, quartz, and nepheline. *Am. J. Sci.* **289**(1), 17–101.

Nagy K. and Lasaga A. (1992) Dissolution and precipitation kinetics of gibbsite at 80 °C and pH 3: the dependence on solution saturation state. *Geochim. Cosmochim. Acta* **56**(8), 3093–3111.

Oelkers E. H. (2001a) An experimental study of forsterite dissolution rates as a function of temperature and aqueous Mg and Si concentrations. *Chem. Geol.* **175**(3–4), 485–494.

Oelkers E. H. (2001b) General kinetic description of multioxide silicate mineral and glass dissolution. *Geochim. Cosmochim. Acta* **65**(21), 3703–3719.

Oelkers E. H. and Gislason S. R. (2001) The mechanism, rates and consequences of basaltic glass dissolution: I. An experimental study of the dissolution rates of basaltic glass as a function of aqueous Al, Si and oxalic acid concentration at 25 °C and pH 3 and 11. *Geochim. Cosmochim. Acta* **65**(21), 3671–3681.

Oelkers E. H. and Schott J. (1995) Experimental study of anorthite dissolution and the relative mechanism of feldspar hydrolysis. *Geochim. Cosmochim. Acta* **59**(24), 5039–5053.

Palmer M. R. and Elderfield H. (1985) Sr isotope composition of sea water over the past 75 Myr. *Nature* **314**(6011), 526–528.

Parkhurst D. L. and Appelo C. A. J. (1999) User's guide to PHREEQC (version 2) – A computer program for speciation, batch-reaction, one-dimensional transport, and inverse geochemical calculations. In *U.S. Geological Survey Water-Resources Investigations Report*, p. 312.

Pearson N. J., Griffin W. L., Alard O. and O'Reilly S. Y. (2006) The isotopic composition of magnesium in mantle olivine: records of depletion and metasomatism. *Chem. Geol. Spec Issue Honour of R.K. O'Nions* **226**(3–4), 115–133.

Petrovic R. (1976) Rate control in feldspar dissolution 2. Protective effect of precipitates. *Geochim. Cosmochim. Acta* **40**(12), 1509–1521.

Petrovich R. (1981) Kinetics of dissolution of mechanically comminuted rock-forming oxides and silicates.1. Deformation and dissolution of quartz under laboratory conditions. *Geochim. Cosmochim. Acta* **45**(10), 1665–1674.

Pistiner J. S. and Henderson G. M. (2003) Lithium-isotope fractionation during continental weathering processes. *Earth Planet. Sci. Lett.* **214**(1–2), 327–339.

Pogge von Strandmann P. A. E., Burton K. W., James R. H., van Calsteren P., Gislason S. R. and Mokadem F. (2006) Riverine behaviour of uranium and lithium isotopes in an actively glaciated basaltic terrain. *Earth Planet. Sci. Lett.* **251**(1–2), 134–147.

Pogge von Strandmann P. A. E., Burton K. W., James R. H., van Calsteren P., Gislason S. R. and Sigfússon B. (2008) The influence of weathering processes on riverine magnesium isotopes in a basaltic terrain. *Earth Planet. Sci. Lett.* **276**(1–2), 187–197.

Pokrovsky O. S. and Schott J. (2000) Kinetics and mechanism of forsterite dissolution at 25 °C and pH from 1 to 12. *Geochim. Cosmochim. Acta* **64**(19), 3313–3325.

Quade J., English N. and DeCelles P. (2003) Silicate versus carbonate weathering in the Himalaya: a comparison of the Arun and Seti River watersheds. *Chem. Geol.* **202**(3–4), 275–296.

Ra K. and Kitagawa H. (2007) Magnesium isotope analysis of different chlorophyll forms in marine phytoplankton using multi-collector ICP-MS. *J. Anal. Atomic Spectrom.* **22**(7), 817–821.

Raymo M. E., Ruddiman W. F. and Froelich P. N. (1988) Influence of Late Cenozoic mountain building on ocean geochemical cycles. *Geology* **16**(7), 649–653.

Richter F. M. and Depaolo D. J. (1988) Diagenesis and Sr isotopic evolution of seawater using data from Dsdp-590b and Dsdp-575. *Earth Planet. Sci. Lett.* **90**(4), 382–394.

Richter F. M., Watson E. B., Mendybaev R. A., Teng F.-Z. and Janney P. E. (2008) Magnesium isotope fractionation in silicate melts by chemical and thermal diffusion. *Geochim. Cosmochim. Acta* **72**(1), 206–220.

Rosso J. J. and Rimstidt J. D. (2000) A high resolution study of forsterite dissolution rates. *Geochim. Cosmochim. Acta* **64**(5), 797–811.

Seitz H.-M., Brey G. P., Lahaye Y., Durali S. and Weyer S. (2004) Lithium isotopic signatures of peridotite xenoliths and isotopic fractionation at high temperature between olivine and pyroxenes. *Chem. Geol.* **212**(1–2), 163–177.

Seyfried W. E., Chen X. and Chan L. H. (1998) Trace element mobility and lithium isotope exchange during hydrothermal alteration of seafloor weathered basalt: an experimental study at 350 °C, 500 bars. *Geochim. Cosmochim. Acta* **62**(6), 949–960.

Stefansson A. and Gislason S. R. (2001) Chemical weathering of basalts, Southwest Iceland: effect of rock crystallinity and secondary minerals on chemical fluxes to the ocean. *Am. J. Sci.* **301**(6), 513–556.

Stillings L. L. and Brantley S. L. (1995) Feldspar dissolution at 25 °C and pH 3 – reaction stoichiometry and the effect of cations. *Geochim. Cosmochim. Acta* **59**(8), 1483–1496.

Stillings L. L., Drever J. I., Brantley S. L., Sun Y. T. and Oxburgh R. (1996) Rates of feldspar dissolution at pH 3–7 with 0–8 mM oxalic acid. *Chem. Geol.* **132**(1–4), 79–89.

Teng F.-Z., Wadhwa M. and Helz R. T. (2007) Investigation of magnesium isotope fractionation during basalt differentiation: implications for a chondritic composition of the terrestrial mantle. *Earth Planet. Sci. Lett.* **261**(1–2), 84–92.

Tipper E. T., Galy A. and Bickle M. J. (2006a) Riverine evidence for a fractionated reservoir of Ca and Mg on the continents: implications for the oceanic Ca cycle. *Earth Planet. Sci. Lett.* **247**(3–4), 267–279.

Tipper E. T., Galy A., Gaillardet J., Bickle M. J., Elderfield H. and Carder E. A. (2006b) The magnesium isotope budget of the modem ocean: constraints from riverine magnesium isotope ratios. *Earth Planet. Sci. Lett.* **250**(1–2), 241–253.

Tipper E., Louvat P., Capmas F., Galy A. and Gaillardet J. (2008) Accuracy of stable Mg and Ca isotope data obtained by MC-ICP-MS using the standard addition method. *Chem. Geol.* **257**(1–2), 65–75.

Tomascak P., Langmuir C., Le Roux P. and Shirey S. (2008) Lithium isotopes in global mid-ocean ridge basalts. *Geochim. Cosmochim. Acta* **72**(6), 1626–1637.

Urey H. C. (1947) The thermodynamic properties of isotopic substances. *J. Chem. Soc. (MAY)* **562**, 581.

Vigier N., Decarreau A., Millot R., Carignan J., Petit S. and France-Lanord C. (2008) Quantifying Li isotope fractionation during smectite formation and implications for the Li cycle. *Geochim. Cosmochim. Acta* **72**(3), 780–792.

Walker J. C. G., Hays P. B. and Kasting J. F. (1981) A negative feedback mechanism for the long-term stabilization of earths surface-temperature. *J. Geophys. Res. Oceans Atm.* **NC86**(10), 9776–9782.

Welch S. A. and Ullman W. J. (1996) Feldspar dissolution in acidic and organic solutions: compositional and pH dependence of dissolution rate. *Geochim. Cosmochim. Acta* **60**(16), 2939–2948.

White A. F. (2003) Natural weathering rates of silicate minerals. In *Treatise on Geochemistry* (eds. H. D. Holland and K. K. Turekian). Pergamon, pp. 133–168.

Wiechert U. and Halliday A. N. (2007) Non-chondritic magnesium and the origins of the inner terrestrial planets. *Earth Planet. Sci. Lett.* **256**(3–4), 360–371.

Wimpenny J., James R., Burton K., Gannoun A., Mokadem F. and Gíslason S. (2010) Glacial effects on weathering processes: new insights from the elemental and lithium isotopic composition of West Greenland rivers. *Earth Planet. Sci. Lett.* **290**(3–4), 427–437.

Wogelius R. A. and Walther J. V. (1991) Olivine dissolution at 25 °C – effects of pH, CO_2, and organic-acids. *Geochim. Cosmochim. Acta* **55**(4), 943–954.

Wogelius R. A. and Walther J. V. (1992) Olivine dissolution kinetics at near-surface conditions. *Chem. Geol.* **97**(1–2), 101–112.

Wolff-Boenisch D., Gislason S. R., Oelkers E. H. and Putnis C. V. (2004) The dissolution rates of natural glasses as a function of their composition at pH 4 and 10.6, and temperatures from 25 to 74 °C. *Geochim. Cosmochim. Acta* **68**(23), 4843–4858.

Wray J. and Daniels F. (1957) Precipitation of calcite and aragonite. *J. Am. Chem. Soc.* **79**(9), 2031–2034.

Young E. D. and Galy A. (2004) The isotope geochemistry and cosmochemistry of magnesium. *Geochem. Non-Traditional Stable Isotopes* **55**, 197–230.

Zhang L. B., Chan L. H. and Gieskes J. M. (1998) Lithium isotope geochemistry of pore waters from Ocean Drilling Program Sites 918 and 919, Irminger Basin. *Geochim. Cosmochim. Acta* **62**(14), 2437–2450.

Zhang Y. and Dawe R. (2000) Influence of Mg^{2+} on the kinetics of calcite precipitation and calcite crystal morphology. *Chem. Geol.* **163**(1–4), 129–138.

Ziegler K., Chadwick O., Brzezinski M. and Kelly E. (2005) Natural variations of 30 Si ratios during progressive basalt weathering, Hawaiian Islands. *Geochim. Cosmochim. Acta* **69**(19), 4597–4610.

Associate editor: Jérôme Gaillardet